Simulating age of air and the distribution of SF_6 in the stratosphere with the SILAM model

Rostislav Kouznetsov[1,2], Mikhail Sofiev[1], Julius Vira[1], and Gabriele Stiller[3]

[1]Finnish Meteorological Institute, Helsinki, Finland
[2]Obukhov Institute for Atmospheric Physics, Moscow, Russia
[3]Karlsruhe Institute of Technology, Karlsruhe, Germany

Correspondence: Rostislav Kouznetsov (Rostislav.Kouznetsov@fmi.fi)

Abstract. The paper presents a comparative study of age of air (AoA) derived with several approaches: a widely used passive tracer accumulation method, the SF_6 accumulation, and a direct calculation of an "ideal age" tracer. The simulations were performed with the Eulerian chemistry transport model SILAM driven with the ERA-Interim reanalysis for 1980-2018.

The Eulerian environment allowed for simultaneous application of several approaches within the same simulation and interpretation of the obtained differences. A series of sensitivity simulations revealed the role of the vertical profile of turbulent diffusion in the stratosphere, destruction of SF_6 in the mesosphere, as well as the effect of gravitational separation of gases with strongly different molar masses.

The simulations reproduced well the main features of the SF_6 distribution in the atmosphere observed by the MIPAS satellite instrument. It was shown that the apparent very old air in the upper stratosphere derived from the SF_6 profile observations is a result of destruction and gravitational separation of this gas in the upper stratosphere and the mesosphere. These processes make the apparent SF_6 AoA in the stratosphere several years older than the "ideal-age" AoA, which, according to our calculations, does not exceed 6-6.5 years. The destruction of SF_6 and the varying rate of emission make SF_6 unsuitable for reliably deriving AoA or its trends. However, observations of SF_6 provide a very useful dataset for validation of the stratospheric circulation in a model with the properly implemented SF_6 loss.

1 Introduction

The age of air (AoA) is defined as the time spent by an air parcel in the stratosphere since its entry across the tropopause (Li and Waugh, 1999; Waugh and Hall, 2002). The distribution of the AoA is controlled by the global atmospheric circulations, first of all, the Brewer-Dobson and the polar circulation. In particular, the temporal variation of AoA has been used as an indicator of the long-term changes in the stratospheric circulation (Engel et al., 2009; Waugh, 2009). AoA has been extensively used for evaluation and comparison of general circulation and chemical transport models in the stratosphere (Waugh and Hall, 2002; Engel et al., 2009).

Simulations of the AoA as defined above have been performed with Lagrangian transport models. The trajectories are initiated with positions distributed in the stratosphere and integrated backwards in time until they cross the tropopause. The time elapsed since the initialization is attributed as age of air at the point of initialization. Moreover, the distribution of the ages

of particles originating from some location can be used to get the age spectrum there. Until recently Lagrangian simulations of AoA did not explicitly account for turbulent mixing in the stratosphere (Eluszkiewicz et al., 2000; Waugh and Hall, 2002; Diallo et al., 2012; Monge-Sanz et al., 2012). Accounting for mixing adds up to two years to the mean AoA in the tropical upper stratosphere (Garny et al., 2014). In Lagrangian models, the mixing can be simulated with random-walk of the particles (Garny et al., 2014), or by inter-parcel mixing (Plöger et al., 2015; Brinkop and Jöckel, 2019).

The Eulerian simulations of AoA can be formulated in several ways. The approaches with an accumulating tracer, whose mixing ratio increases linearly in the troposphere, were used in a comprehensive study by Krol et al. (2018) and several studies before (e.g. Eluszkiewicz et al., 2000; Monge-Sanz et al., 2012). Another approach is to simulate a steady distribution of a decaying tracer, such as ^{221}Rn, emitted at the surface at a constant rate (Krol et al., 2018). Besides that, a special tracer that is analogous to the Lagrangian clock has been used. The tracer appears in the literature under names "clock-type tracer"(Monge-Sanz et al., 2012) or "ideal age" (Waugh and Hall, 2002). The ideal age has a constant rate of increasing of mixing ratio everywhere, except for the surface where it is continuously forced to zero. Similar tracers have been long used to simulate the transport times of oceanic water (e.g. England, 1995; Thiele and Sarmiento, 1990).

Direct observations of the age of air, as it is defined above, are not possible; therefore AoA is usually derived from the observed mixing ratios of various tracers with known tropospheric mixing ratios and lifetimes (Bhandari et al., 1966; Koch and Rind, 1998; Jacob et al., 1997; Patra et al., 2011), or from the long-living tracers with known variations in the tropospheric mixing ratios. The studies published to-date used carbon dioxide CO_2 (Andrews et al., 2001; Engel et al., 2009), nitrous oxide N_2O (Boering et al., 1996; Andrews et al., 2001), sulphur hexafluoride SF_6 (Waugh, 2009; Stiller et al., 2012), methane CH_4 (Andrews et al., 2001; Remsberg, 2015), and various fluorocarbons (Leedham Elvidge et al., 2018).

For accumulating tracers, the mean AoA at some point in the stratosphere is calculated as a lag between the times when a certain mixing ratio is observed near the surface and at that point. The lag time is equivalent to the mean AoA defined above only in the case of the strictly linear growth and the uniform distribution of the tracer in the troposphere (Hall and Plumb, 1994).

In reality, there is no tracer whose mixing ratio in the troposphere grows strictly linearly. The violation of the assumption of the linear growth leads to biases in the resulting AoA distribution and its trends. It has been pointed out that the increasing growth rates of CO_2 and SF_6 lead to a low-bias of AoA and its trends, and make these tracers ambiguous proxies of the AoA (Garcia et al., 2011). Various corrections have been applied in several studies (Hall and Plumb, 1994; Waugh and Hall, 2002; Engel et al., 2009; Stiller et al., 2012; Leedham Elvidge et al., 2018) to deduce the "true" AoA from observations of tracers with the increasing growth rates. The effect of the correction method on the AoA estimates has not been investigated and must be considered as a source of uncertainty in the resulting estimates. Thus, Garcia et al. (2011) concluded that accounting for the biases in the trend estimates due to varying growth rates would likely require uniform and continuous knowledge of the evolution of the trace species, which is not available from any existing observational dataset. Recently Leedham Elvidge et al. (2018) showed a minor sensitivity of the AoA to the choice of the correction method, however without detailed analysis of the assumptions behind these methods. For similar problem with the ages of oceanic water it has been shown (Waugh et al.,

2003) that in case of a inhomogeneously growing tracer the tracer age is strongly influenced by the shape of the transient time distribution (TTD, also known as the "age spectrum") at the particular location and time.

Another major source of uncertainty in the observational AoA is the violation of conservation of the tracer due to sources and sinks, such as oxidation of carbon monoxide and methane for CO_2 or mesospheric destruction for SF_6. The mesospheric sink of SF_6 leads to the "over-aging" especially pronounced in the area of the polar vortices. The magnitude of the over-aging was estimated as at least two years Waugh and Hall (2002). Besides being visible in many evaluations, e.g. Stiller et al. (2012, Fig. 4), Kovács et al. (2017, Fig. 8), the over-aging of the polar winter stratospheric air was studied by Ray et al. (2017, Fig. 4) within the dedicated exercise.

The simulations of SF_6 and the AoA in the atmosphere with WACCM model (Kovács et al., 2017) have also reproduced the effect of over-aging. However, its magnitude was much smaller than that inferred from the SF_6 retrievals of the limb-viewing MIPAS instrument operated on-board of the Envisat satellite in 2002-2012 (Stiller et al., 2012), and from the *in-situ* observations of the ER-2 aircraft (Hall et al., 1999). Kovács et al. (2017) offered two possible reasons for the discrepancy: either SF_6 loss is still underestimated in WACCM, or MIPAS SF_6 observations are low biased above $\sim 20\,\mathrm{km}$. Neither of the cases have been analysed in depth which leaves the status of MIPAS, currently the richest observational dataset for the stratospheric SF_6, unclear.

The aim of the present study is to provide self-consistent simulations of spatio-temporal distribution of the AoA and of the SF_6 mixing ratio in the troposphere and the stratosphere during last 39 years. The main modelling tool is the Eulerian chemistry transport model SILAM (System for Integrated modeLling of Atmospheric coMposition). The stratospheric balloon observations and retrievals of the limb-viewing MIPAS instrument said above are used for validation of the simulated distribution.

With these simulations we

- compare different methods of estimating the AoA and quantify the inconsistencies in the AoA and its trends arising from violations of the underlying assumptions behind each method
- analyze the causes of the discrepancies in the upper stratosphere between different methods of deriving the AoA
- provide a solid basis for further studies of stratospheric circulation with observations of various trace gases and for studies of climate effects of SF_6

The paper is organized as follows. Sec. 2 gives an overview of the modelling tools and the modelling and observational data used for the study. Sec. 3 describes the developments made for SILAM in order to perform the simulations: vertical eddy diffusivity parametrisation in the stratosphere and the lower mesosphere, and the SF_6 destruction parametrization, as well as the model configuration used for the study. The sensitivity tests and evaluation of the simulations against the MIPAS retrievals and stratospheric-balloon measurements of SF_6 mixing ratios are given in Sec. 4. Sensitivity of the AoA and its trends to the simulation setup and the choice of particular SF_6 tracer as an AoA proxy is studied in Sec. 5. The uncertainties of the used modelling approach and implications of AoA derived from SF_6 tracer discussed in Sec. 6. The results are summarised in Sec. 7.

2 Methods and input data

2.1 SILAM model

SILAM (System for Integrated modeLling of Atmospheric coMposition, http://silam.fmi.fi) is an offline 3D chemical-transport model. SILAM features a mass-conservative and positive-definite advection scheme that makes the model suitable for long-term runs (Sofiev et al., 2015). The model can be run at a range of resolutions starting from a kilometer scale in limited-area and up to a global coverage. The vertical structure of the modelling domain consist of stacked layers starting from the surface. The layers can be defined either in z- or hybrid sigma-pressure coordinates. The model can be driven with a variety of NWP- (numerical weather prediction) or climate models.

The global 3D simulations of atmospheric transport for a variety of tracers representing AoA and SF_6 (see Sec. 3.4 for details) were performed with SILAM for the years 1980-2018 with the global lon-lat grid of $1.44°$x$1.44°$ cells (250x123 grid cells plus polar closures) and 60 hybrid sigma-pressure layers starting from the surface. The uppermost layer was between pressures of 0.1 and 0.2 hPa whereas other layer's bounds corresponded to the half-levels of the meteorological driver - the ERA-Interim reanalysis (Sec. 2.2). The model time step was 15 minutes and the output consisted of daily mean 3D concentrations of the tracers and air density. Emission data were taken from the SF_6 emission inventory (Rigby et al., 2010), which was extrapolated till 2016 as described in Sec. 3.4. Physical-chemical transformations of the SF6-related tracers required developments described in Sec. 3.3.

In order to accurately model the AoA and the needed tracers, the vertical diffusion part of the transport scheme of SILAM has been refined to account for gravitational separation. In addition, several tracers with corresponding transformation routines have been implemented into the model. The SILAM configuration, used for the present study is described in Sec. 3.4.

2.2 ECMWF ERA-interim reanalysis

The ERA-Interim reanalysis of the European Centre for Medium-range Weather Forecasts (ECMWF) had been used as a meteorological driver for our simulations. The dataset has T255 spectral resolution and covers the whole atmosphere with 60 hybrid sigma-pressure levels having the uppermost layer from 0.2 to 0 hPa with nominal pressure of 0.2 hPa (Dee et al., 2011). The reanalysis uses a 12-h data assimilation cycle, and the forecasts are stored with a 3-hour time step. We used the fields retrieved from the ECMWF's MARS archive on a lon-lat grid 500x250 points with the step of 0.72 degrees. The four forecast times (+3h, +6h, +9 h and +12h) were used from every assimilation cycle to obtain a continuous dataset with 3-hour time step. To drive the dispersion model, the data on horizontal winds, temperature and humidity for 1980-2018 were used.

Since the resolution of the driving meteorology was twice higher than that of SILAM, the meteorological input for both cell-interface for winds and cell mid-points for other parameters (surface pressure, temperature and humidity) was available without interpolation. The gridded ERA-interim fields are, however, a result of reprojection of the original meteorological fields computed as spherical harmonics. Moreover, the difference in the top-most layer of the ERA-Interim and SILAM required vertical reprojection at the top of the domain. Together with limited precision of the gridded fields in the GRIB files they caused some inconsistency between the surface-pressure tendencies and the vertically-integrated air-mass fluxes calculated

from the meteorological fields in SILAM. Albeit small, such inconsistencies cause spurious variations in wind-field divergence that might result in gradual accumulation of errors in the tracer mixing ratios. To maintain strict global and local air-mass budget throughout the run, the wind fields were adjusted by distributing the residuals of pressure tendency and vertically-integrated horizontal air-mass fluxes as a correction to the horizontal winds, as suggested by Heimann and Keeling (1989). The correction was, a most, of the order of centimeters per second, which is comparable to the precision of the input wind fields. The vertical wind component was then re-diagnosed from the divergence of the horizontal air-mass fluxes for the SILAM layers as described in (Sofiev et al., 2015). Validity of this procedure was demonstrated by its authors Heimann and Keeling (1989) and its applicability to the current case was confirmed in the section 5.2 by comparison with another model simulations driven by ERA-Interim (Diallo et al., 2012).

The ERA-interim reanalysis has been used earlier for Lagrangian simulations of AoA (Diallo et al., 2012) and found to provide ages that agree with those inferred from *in-situ* observations in the lower stratosphere.

2.3 MIPAS observations of SF_6

To evaluate the results of the SF_6 modelling we used the data from the MIPAS instrument operated on-board of Envisat satellite in 2002-2012. MIPAS was a limb-sounding Fourier transform spectrometer with a high spectral resolution measuring in the infrared part of spectrum. Due to its limb geometry, the instrument provided good vertical resolution of the derived trace gas profiles and showed high sensitivity to low-abundant species around the tangent point. Along the orbit path, MIPAS measured a profile of atmospheric radiances about every $400\,\mathrm{km}$ with an altitude coverage, in its nominal mode, from 6 to 70 km. The vertical sampling was $1.5\,\mathrm{km}$ in the lower part of the stratosphere (up to $32\,\mathrm{km}$) and $3\,\mathrm{km}$ above, with a vertical field of view covering $3\,\mathrm{km}$ at the tangent point. Over a day, about 1300 profiles along 14.4 orbits were measured, covering all latitudes up to the poles at sunlit and dark conditions. The vertical distributions of trace gases were derived from the radiance profiles by an inversion procedure, fitting simulated spectra to the measured ones while varying the atmospheric state parameters.

The retrieval of SF_6 is based on the spectral signature of this species in the vicinity of $10.55\,\mu\mathrm{m}$ wavelength and is described in Stiller et al. (2008, 2012); Haenel et al. (2015). In the current study, we use an updated version of the SF_6 data (compared to the one described in Haenel et al. (2015)) called V5H/R_SF6_21/224/225. The new algorithm uses the new absorption cross-section data on the SF_6 and a new CFC-11 band in the vicinity of the SF_6 signature by Harrison (2018) instead of the older cross section data by Varanasi et al. (1994). The updated version provides up to $0.6\,\mathrm{pmol/mol}$ higher SF_6 mixing ratios in the upper part of the stratosphere (above $30\,\mathrm{km}$) than the old versions and is closer to independent reference data. Note that whilst we regard this newer version of MIPAS SF_6 data as an improvement, it has not yet been reported in a publication, and on that basis is subject to uncertainty.

The retrieved profiles are sampled on an altitude grid spaced at $1\,\mathrm{km}$, whereas the actual resolution of the profiles is between 4 and $10\,\mathrm{km}$ for altitudes below $30\,\mathrm{km}$. The retrievals are supplemented with averaging kernels and error covariance matrices describing the uncertainties due to random noise in the radiance measurements, hereinafter referred as measurement noise error or target noise error or retrieval noise error. This error component, which is normally in the order of 10% of the retrieved value, is fully uncorrelated from profile to profile, and therefore virtually cancels out when averaged over a large number of profiles.

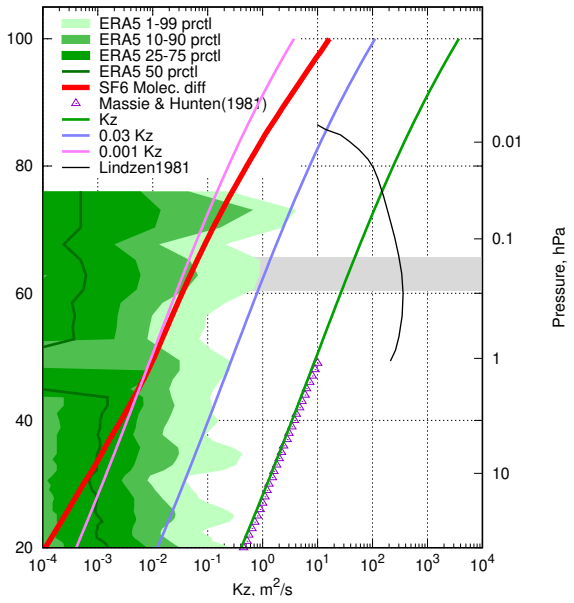

Figure 1. Vertical profiles of diffusion coefficients. The distribution of the ERA5 profiles of the "mean turbulent diffusion coefficient for heat" parameter, molecular diffusivity for SF_6 in the standard atmosphere, and the three prescribed Kz profiles. The eddy diffusion profile due to breaking gravity waves (after Lindzen, 1981) is given for the reference.

In contrast, there exist systematic error components that are fully correlated between the profiles. Their assessment is difficult and depends on the knowledge about sources of systematic errors. Stiller et al. (2008) has assessed them to be in the order of 10% at 60 km, and 4% at 30 km. These error components have to be considered when comparisons of monthly or seasonal means with other data are performed.

3 SILAM developments

Destruction of the atmospheric SF_6 occurs at altitudes above 60 km (Totterdill et al., 2015) that fall within the topmost layer of the ERA-Interim. The exchange processes in the upper stratosphere and lower mesosphere have to be adequately parameterized together with the destruction process. In our simulations we have suppressed the transport of SF_6 with mean wind through the modelling domain top ($0.1\,hPa$, 65 km) and parameterized the SF_6 loss due to the eddy and molecular diffusion towards the altitudes where the destruction occurs. In this section we introduce the set of parametrizations that were implemented in SILAM for this study.

3.1 Eddy diffusivity

Large variety of vertical profiles for eddy diffusivity in the stratosphere and the lower mesosphere can be found in literature. In many studies in 1970-s – 1980-s the vertical profiles were derived from observed tracer concentrations neglecting the mean

transport. Most studies suggested that the vertical eddy diffusion has a minimum of 0.2-0.5 m^2/s (Pisso and Legras, 2008) at 15-20 km agreeing quite well to the ones derived from the radar measurements in the range of 15-20 km Wilson (2004). Above that altitude K_z was suggested to gradually increase by about 1.5 orders of magnitude towards 50 km due to breaking gravity waves (Lindzen, 1981).

The theoretical estimates of the effective exchange coefficients considering the layered and patchy structure of stratospheric turbulence suggest 0.5–2.5 m^2/s for the upper troposphere and 0.015–0.02 m^2/s for the lower stratosphere (Osman et al., 2016), which is about an order of magnitude lower than the estimates above.

The values of the eddy exchange coefficient at heights of 10-20km estimated from the high-resolution balloon temperature measurements (Gavrilov et al., 2005) are ~ 0.01 m^2/s with no noticeable vertical variation. It is not clear, however, how representative the derived values are for UTLS in general. We could not find any reliable observations of vertical diffusion in a range of 30-50 km.

The parameterisation for vertical eddy diffusivity above the boundary layer used in SILAM has been adapted from the IFS model of the European Centre for Medium-range Weather Forecasts (ECMWF, 2015). However, in the upper troposphere the predicted eddy diffusivity is nearly zero. For numerical reasons a lower limit of 0.01 m^2/s is set for K_z in SILAM. Our sensitivity tests have shown that long-term simulations are insensitive to this limit as long as it is low enough (see results and discussion). The K_z in the stratosphere is routinely set to the limiting value with relatively rare peaks, mostly in UTLS. Such scheme essentially turns off turbulent diffusion in the stratosphere. Same is true for the recent ERA5 reanalysis dataset (Copernicus Climate Change Service (C3S), 2017) that provides the values of K_z among other model-level fields: the eddy diffusion routinely falls below the molecular diffusivity above 40 km (Fig. 1).

As a reference for this study, we took a tabulated profile of Hunten (1975), as it was quoted by Massie and Hunten (1981). The original profile covers the range up to 50 km, and the extrapolation up to 80 km matches the theoretical estimates by (Lindzen, 1981) and by Allen et al. (1981). We approximate the profile as a function of pressure in the range of $100 - 0.01\,\mathrm{hPa}$ $(15 - 60\,\mathrm{km})$:

$$K_z(p) = 8\,\mathrm{m}^2/\mathrm{s}\left(\frac{1\,\mathrm{hPa}}{p}\right)^{0.75}. \tag{1}$$

The approximated profile was stitched with the default SILAM profile with a gradual transition within an altitude range of $10 - 15\,\mathrm{km}$ to keep the tropospheric dispersion intact. This profile gives values of K_z 3 – 6 orders of magnitude higher than the ones provided by the ERA5 reanalysis (Fig. 1), and 1-2 orders of magnitude higher than the estimates of (Legras et al., 2005).

In order to cover the range of K_z between the ERA5 profiles and the reference one (1) we used two intermediate profiles obtained by scaling the reference one with factors 0.03 and 0.001. The three prescribed eddy-diffusivity profiles are hereinafter referred as “1Kz”, “0.03Kz”, and “0.001Kz”, respectively. The dynamic eddy-diffusivity profile adopted from the ECMWF IFS is referred to as “ECMWF Kz”. In all simulations, the parameterization of K_z in the troposphere is the same and linear transition from the SILAM K_z to the prescribed one occurs in the altitude range of $10 - 15\,\mathrm{km}$.

3.2 Molecular diffusivity and gravitational separation

In tropospheric and stratospheric CTMs, gaseous admixtures are transported as tracers, i.e. advection and turbulent mixing do not depend on the species properties, whereas the molecular diffusion is negligible. Models that cover the mesosphere, such as WACCM (Smith et al., 2011), account for molecular diffusion explicitly. Since some of the K_z parametrizations of the previous section often result in values below the molecular diffusivity, the parametrization of molecular diffusion has been implemented in SILAM.

The molecular diffusivity of SF_6 in the air at temperature $T_0 = 300$ K and pressure $p_0 = 1000\,\mathrm{hPa}$, is $D_0 = 1 \times 10^{-5}\,\mathrm{m\,s^{-2}}$ (Marrero and Mason, 1972, Table 22). The diffusivity at different temperature T and pressure p is given by:

$$D = D_0 \frac{p_0}{p} \left(\frac{T}{T_0} \right)^{3/2}, \tag{2}$$

see e.g. Cussler (1997). The vertical profile of molecular diffusivity in the US standard atmosphere (NOAA et al., 1976) is shown in (Fig. 1). Note that the value for the reference diffusivity of SF_6 used in this paper is about a half of the one used in simulations with WACCM by Kovács et al. (2017). The reason is that WACCM uses a universal parametrization (Smith et al., 2011, Eq. 7 there) for all compounds. That parametrization relies solely on molecular mass of a tracer and does not account for e.g. the molecule collision radius. The latter is about twice larger for SF_6 than for most of stratospheric tracers. Thus, for this study we use the value from Marrero and Mason (1972), which results from fitting laboratory data for diffusion of SF_6 in the air.

The vertical diffusion transport velocity of admixture with number concentration $\tilde{n}$ and molecular mass $\tilde{\mu}$ in neutrally-stratified media is given by (Mange, 1957):

$$w = -D \left[\frac{1}{\tilde{\mu}} \frac{\partial \tilde{\mu}}{\partial z} + \left(\frac{\tilde{\mu}}{\mu} - 1 \right) \frac{\mu g}{kT} \right], \tag{3}$$

where μ is molecular masses of air, g – acceleration due to gravity, k is the Boltzmann constant, and T is temperature. With ideal gas law $p = nkT$, in which p is pressure, and n is number concentration, and static law $dp/dz = -g\rho$, where $\rho = \mu n$ is air density, the equation (3) can be reformulated in terms of admixture mixing ratio $\xi = \tilde{n}/n$ and pressure. Then the vertical gradient of the equilibrium mixing ratio will be:

$$\frac{\partial \xi}{\partial p} = \left(\frac{\tilde{\mu}}{\mu} - 1 \right) \frac{\xi}{p}. \tag{4}$$

It is non-zero for an admixture of a molecular mass different from one of the air. Integrating the gradient (4) over vertical, one can obtain that the equilibrium mixing ratios ξ_1 and ξ_2 at two levels with corresponding pressures p_1 and p_2 are related as:

$$\frac{\xi_1}{\xi_2} = \left(\frac{p_1}{p_2} \right)^{\tilde{\mu}/\mu - 1}. \tag{5}$$

For heavy admixtures, such as SF_6 ($\tilde{\mu} = 0.146$ kg/mole) the equilibrium gradient of a mixing ratio is substantial. For example, the difference of the equilibrium mixing ratio of SF_6 between 0.1 and $0.2\,\mathrm{hPa}$ is a factor of 16.

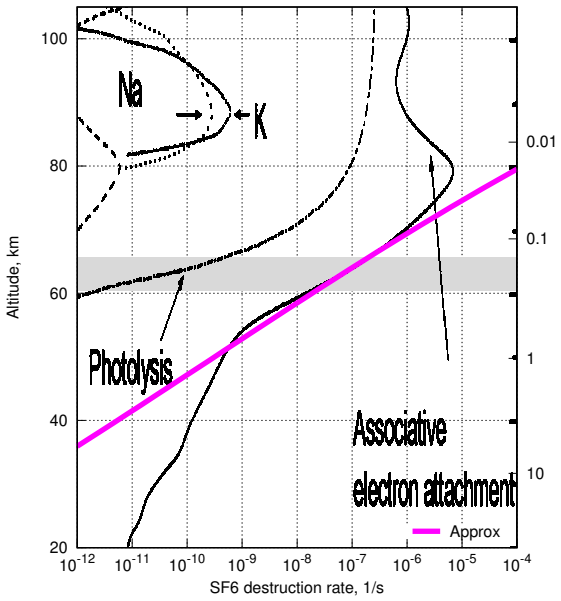

Figure 2. The vertical profiles of SF_6 destruction rate (after Totterdill et al., 2015) and its approximation in range of 55-75 km, given by Eq. (6).

In most of the atmosphere, the effect of gravitational separation is insignificant due to the overwhelming effect of other mixing mechanisms, whereas in the upper stratosphere the molecular diffusivity may become significant. Therefore, in the upper stratosphere heavy gases can no longer be considered as tracers and the molecular diffusion should be treated explicitly. The effect of gravitational separation of nitrogen and oxygen isotopes in the stratosphere has been observed (Ishidoya et al., 2008, 2013; Sugawara et al., 2018), however for isotopes the ratio of masses is relatively small, so the observed differences were also small (up to 10^{-5}). For SF_6 the molecular mass difference is much larger.

In order to enable the gravitational separation in SILAM we have introduced the molecular diffusion mechanism, which can be enabled along with the turbulent diffusion scheme. The exchange coefficients due to molecular diffusion between the model layers are pre-calculated according to Eq. (3) discretized for the given layer structure for each species according to its diffusivity and molar mass. The US standard atmosphere (NOAA et al., 1976) was assumed for the vertical profiles of temperature and air density during pre-calculation of the exchange coefficients. The exchange has been applied throughout the domain at every model time step with a simple explicit scheme.

3.3 SF_6 destruction

Estimates of AoA from the SF_6 tracer rely on the assumption of it being a passive tracer. SF_6 is indeed essentially stable in the troposphere and the stratosphere. IPCC (2013, Sec 8.2.3.5) mentions that photolysis in the stratosphere as the main mechanism of SF_6 loss, however without any reference to original studies. The statement is probably taken from Ravishankara

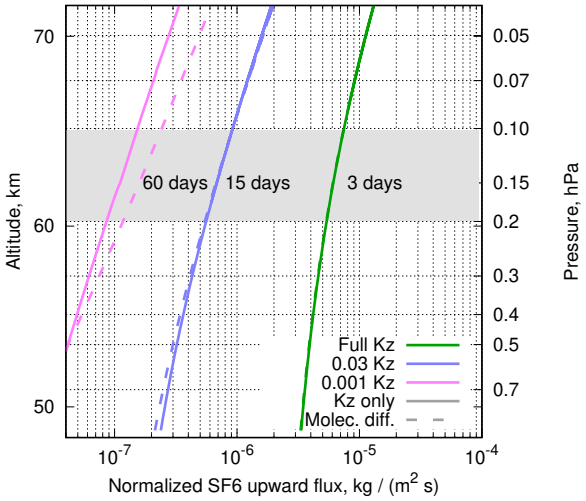

Figure 3. Vertical profiles of steady-state upward flux of SF_6 normalized with mass mixing ratio $F(p)/\xi(p)$, for eddy diffusivity and lifetime profiles given by (1) and (6). The upper model layer of SILAM and effective lifetimes of SF_6 there due to the destruction in the mesosphere for different Kz profiles are given.

et al. (1993). Reddmann et al. (2001) pointed at associative electron attachment in the upper stratosphere and mesosphere as the main destruction mechanism for SF_6 below 80 km. The recent study of Totterdill et al. (2015) gives some 1-2 order of magnitude slower rates of electron attachment, however keeping it the dominant mechanism of the SF_6 destruction in the altitude range up to 100 km. The highest destruction rate of $1 \times 10^{-5}\,\mathrm{s}^{-1}$ occurs at the altitude of 80 km (Fig. 2). An important feature of this profile is that the destruction rate becomes significant above the top of our modelling domain ($0.1\,\mathrm{hPa}$, 65 km). The ERA-Interim meteorological fields have the uppermost level at $0.1\,\mathrm{hPa}$ and do not resolve the vertical structure of the atmosphere above that level. In order to assess the loss of SF_6 we have to parameterise the combined effect of the SF_6 transport through the $0.1\,\mathrm{hPa}$ and its destruction. Then the resulting fluxes can be applied as the upper boundary condition for our simulations.

As an approximation to the vertical profile of the destruction rate in an altitude range of 50–80 km we have fitted the corresponding part of the curve in Fig. 9a of Totterdill et al. (2015) with a power function of pressure (magenta line in Fig. 2):

$$\frac{1}{\tau} = 3 \times 10^{-8}\,\mathrm{s}^{-1} \left(\frac{0.2\,\mathrm{hPa}}{p} \right)^3, \tag{6}$$

where τ is the lifetime of SF_6 at the altitude corresponding to pressure p.

The topmost level of the ERA-Interim meteorological dataset is located at $0.1\,\mathrm{hPa}$, which is below the layer where the destruction of SF_6 occurs. Therefore we have to put a boundary condition to our simulations to account for the upward flux of SF_6 through the upper boundary of the simulation domain. For that we assume that SF_6 distribution above the computational domain top is in equilibrium with the destruction and the vertical flux.

Assuming the profiles for $K_z(p)$ and the SF_6 lifetime $\tau(p)$ are given by (1) and (6), one can obtain a steady-state distribution of the mass-mixing ratio ξ of SF_6 due to destruction in the mesosphere at any point where both (1) and (6) are valid and vertical advection is negligible. The latter assumption implies that the diffusive vertical flux overwhelms the advective one. The validity and implications of neglecting the regular vertical transport are discussed below. The steady-state profile of ξ can be obtained from a solution of the steady-state diffusion equation with a sink:

$$\frac{\partial \xi}{\partial t} = g\frac{\partial}{\partial p}(F) - \frac{\xi}{\tau(p)} = 0, \tag{7}$$

where $\rho(p)$ is air density, and g is acceleration due to gravity, and the upward flux of SF_6 is given by

$$F(p) = g\rho^2 K_z(p)\frac{\partial \xi}{\partial p} \tag{8}$$

The above equation was solved numerically as a boundary value problem with unit mixing ratio at a height of $1\,\mathrm{hPa}$ and vanishing flux $F(p)$ at $p = 0$ for the set of Kz profiles. The shooting method with bisection was used to get the steady-state profiles of $\xi(p)$ and $F(p)$, corresponding to $\xi(1\,\mathrm{hPa}) = 1$. For all considered cases the flux $F(p)$ decreased by several orders of magnitude already at the level of a few Pa, i.e. below the maximum of the depletion profile of Totterdill et al. (2015), indicating that particular shape of $\tau(p)$ above that level does not influence the fluxes at the domain top ($0.1\,\mathrm{hPa}$). The steady-state upward flux of SF_6 $F(p)$ normalized with the corresponding mixing ratio at each pressure $F(p)/\xi(p)$, for the three test profiles of K_z is shown in Fig. 3 with solid lines.

The gravitational separation can be accounted for by introducing a term responsible for molecular diffusion and its equilibrium state (4)into the vertical flux Eq. (8) :

$$F(p) = g\rho^2 K_z(p)\frac{\partial \xi}{\partial p} + g\rho^2 D(p)\left(\frac{\partial \xi}{\partial p} - \frac{\tilde{\mu}-\mu}{\mu}\frac{\xi}{p}\right) \tag{9}$$

The profiles of $F(p)/\xi(p)$ resulting from $F(p)$ in equation (7) are given in Fig. 3 with dashed lines. The magnitude of $F(p)/\xi(p)$ gives an equivalent regular vertical air-mass flux that would result in the same vertical flux of SF_6 if it were passive and non-diffusive. The equivalent regular vertical velocity ω_{eq} (in units of the Lagrangian tendency of a parcel pressure due to vertical advection) can be expressed as:

$$\omega_{eq} = -gF(p)/\xi(p). \tag{10}$$

Accounting for molecular diffusion may either enhance or reduce the upward flux of SF_6 in the model. Along with setting the equilibrium state with the bulk of a heavy admixture being in the lower layers, molecular diffusion provides additional means for transport to the upper layers where the destruction occurs. For very low eddy diffusivities, the molecular diffusion is a sole mechanism of the upward transport of SF_6 towards depletion layers. For higher eddy diffusivity the effect of molecular diffusion and gravitational separation becomes negligible.

For the model consisting of stacked well-mixed finite layers, the loss of SF_6 from the topmost layer due to the steady upward flux would be proportional to the SF_6 mixing ratio in the layer. This loss of mass is equivalent to a linear decay of SF_6 in the

layer at a rate

$$\tau^{-1} = g\frac{F(p)}{\xi(p)\Delta p}, \tag{11}$$

where Δp is pressure drop in the layer.

In the upper layer of our simulations (between 0.1 hPa and 0.2 hPa, grey rectangle in Fig. 3), the SF_6 lifetime τ due to turbulent diffusion is about 3 days for K_z of Eq.(1). After scaling the $K_z(p)$ profile with factors of 0.03, and 0.001 one gets the lifetimes of 15 and 60 days, respectively. Noteworthy, the molecular diffusion sets the upper limit to the SF_6 lifetime in the topmost model layer: it can not be longer than 60 days for the 0.1 - 0.2 hPa layer. Close to this regime, the system becomes insensitive to the actual profile and values of the turbulent diffusion coefficient. The loss of SF_6 through the domain top was implemented as a linear decay of SF_6 in the topmost model layer, at a rate corresponding to the $K_z(p)$ profile used in each simulation.

3.4 Simulated tracers

SILAM performs the 3D transport by means of a dimension split: transport along each dimension is performed separately as 1D transport. To minimize the inconsistency between the tracer transport and air-mass fluxes caused by the dimension split at finite time step, the splitting sequence has been inverted at each time step. The residual inconsistency was resolved by using a separate unity tracer, which was initialized to the constant mass mixing ratio of 1 at the beginning of a simulation. Should advection be perfect, the concentration of the unity tracer would be equivalent to air density (mixing ratio would stay equal to 1). The mixing ratios of the simulated tracers were then evaluated as a ratio of the tracer mass in a cell to the mass of the unity tracer.

In order to assess the effects of gravitational separation and destruction on the atmospheric distribution of SF_6, we used four tracers: SF_6 as a passive tracer "sf6pass", SF_6 with gravitational separation but no destruction "sf6nochem" (no chemistry), SF_6 with destruction but no gravitational separation "sf6nograv", and SF_6 with both gravitational separation and destruction in the upper model level "sf6".

All SF_6 tracers had the same emission according to the SF_6 emission inventory (Rigby et al., 2010). The inventory covers 1970-2008, and was extrapolated with a linearly growing trend of $0.294\,\mathrm{Gg/y/y}$ until July 2016. The last 2.5 years were run without the SF_6 emissions to evaluate its destruction rate. Note that the emission extrapolation gives for 2016 $9.4\,\mathrm{Gg/y}$, which is somewhat higher than later estimate $8.8\,\mathrm{Gg/y}$ (Engel et al., 2018).

Besides the four SF_6 tracers we used a "passive" tracer emitted uniformly at the surface at constant rate during the whole simulation time and an "ideal age" tracer. The "ideal age" tracer is defined as a tracer whose mixing ratio ξ_{ia} obeys continuity equation (Waugh and Hall, 2002):

$$\frac{\partial \xi_{\mathrm{ia}}}{\partial t} + \mathcal{L}(\xi_{\mathrm{ia}}) = 1, \tag{12}$$

(where $\mathcal{L}$ is the advection-diffusion operator), and boundary condition $\xi_{\text{ia}} = 0$ at the surface. The "ideal age" tracer is transported as a regular gaseous tracer and updated at every model time step Δt with the unity tracer correction:

$$M_{\text{ia}} \mapsto \begin{cases} 0, & \text{at lowest layer,} \\ M_{\text{ia}} + M_{\text{unity}} \Delta t, & \text{otherwise,} \end{cases} \tag{13}$$

where M_{ia} and M_{unity} are masses of the "ideal age" tracer and of the unity tracer in the grid cell. The mixing ratio of the "ideal age" tracer is a direct measure of the mean age of air in a cell, so the tracer is a direct Eulerian analog of the time-tagged Lagrangian particles with clock reset at the surface. Note that the AoA derived from the "ideal age" tracer and AoA from a passive tracer with a linearly-growing near-surface mixing ratio are equivalent (Waugh and Hall, 2002), and implementation of both provides a redundancy needed to ensure self-consistency of our results.

The simulations were performed with four eddy diffusivity profiles described in Sec. 3.1 and the corresponding destruction rates of "sf6" and "sf6nograv" tracers in the uppermost model layer. All runs were initialized with the mixing ratios from the final state of a special initialization run. The initialization simulation with "0.1Kz" eddy diffusivity was started from 1970 with zero fields for all tracers, except for unity tracer that was set to unity mixing ratio. The simulation used 1970-1989 emissions for $\mathrm{SF_6}$ species from the same inventory as for the main runs (Rigby et al., 2010), and driven with the twice repeated ERA-Interim meteorological fields for 1980-1989. The mixing ratios of all $\mathrm{SF_6}$ tracers at the end of the initialization run were scaled to match the total $\mathrm{SF_6}$ burden of $20.17\,\mathrm{Gg}$ in 1980 (Levin et al., 2010).

4 Sensitivity and validation of $\mathrm{SF_6}$ simulations

4.1 Gravitational separation and mesospheric depletion

To evaluate the relative importance of gravitational separation and mesospheric depletion and their effect on the $\mathrm{SF_6}$ concentrations we compared the simulations for the $\mathrm{SF_6}$ tracers and evaluated the relative reduction of the $\mathrm{SF_6}$ content in the stratosphere due to these processes. As a conservative estimate of the reduction, we evaluated the relative differences between the tracers in the latitude belt of 70-85S, since both processes have the most pronounced effect in the southern polar vortex, where the downwelling of Brewer-Dobson circulation is the strongest.

Hereafter we quantify the relative difference between atmospheric contents of two $\mathrm{SF_6}$ tracers "X" and "Y" as:

$$\Delta(\text{"X"}, \text{"Y"}) = 2\frac{\xi_{\text{X}} - \xi_{\text{Y}}}{\xi_{\text{X}} + \xi_{\text{Y}}} \cdot 100\%. \tag{14}$$

The relative differences for the $\mathrm{SF_6}$ tracers in the Southern polar region (70-85S) simulated with two extreme K_z profiles is given in Fig. 4 as a function of time and altitude. Noteworthy, every 5% of the decrease of $\mathrm{SF_6}$ with respect to its passive counterpart correspond to about one year of a positive bias in AoA derived from the $\mathrm{SF_6}$ mixing ratios.

The reduction of the $\mathrm{SF_6}$ content due to gravitational separation if the mesospheric depletion is disabled is given by the relative difference of "sf6nochem" and "sf6pass" (Fig. 4ab). Expectedly, the effect of gravitational separation is most pronounced for the case of low eddy diffusivity ("0.001 Kz"), and the reduction of $\mathrm{SF_6}$ in the altitude range of 30–50 km reaches 2 – 5 %. In the case of strong mixing, the effect of separation is about 1 %.

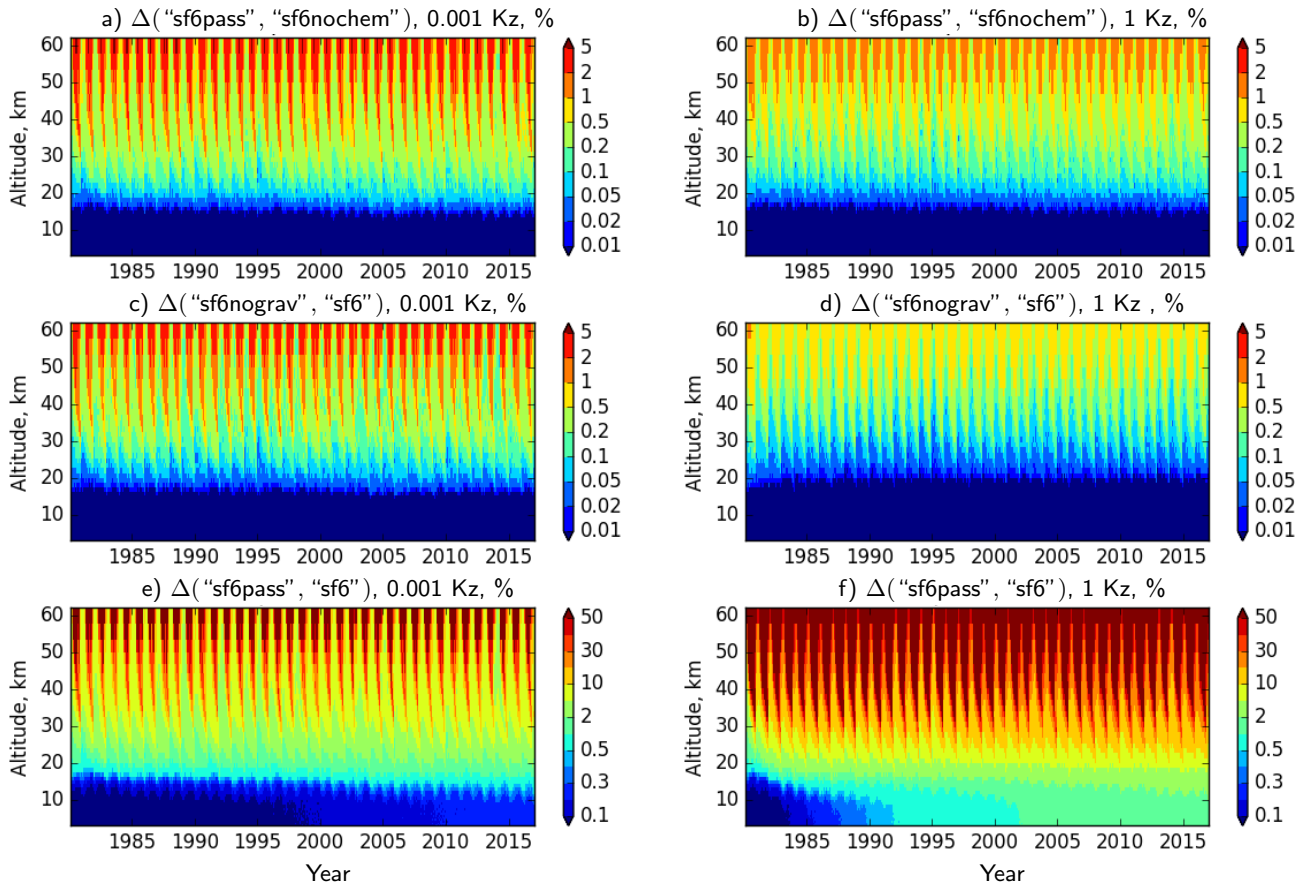

Figure 4. The relative reduction of the SF_6 content (in %) at 70-85S due to gravitational separation with (a, b) and without (c, d) depletion, and due to combined effect of depletion and separation (e, f) at two extreme Kz cases. Note different color scales for e) and f).

The reduction of the SF_6 content due to gravitational separation in presence of stratospheric depletion is given by the relative difference of "sf6nograv" and "sf6" tracers. The effect of the separation for low K_z is very similar between the depletion and no-depletion cases (Fig. 4c vs. Fig. 4a). Depletion reduces the effect of the gravitational separation for high K_z (Fig. 4b vs Fig. 4d). Regardless depletion, stronger K_z reduces the effect of the gravitational separation, however the latter is still non-negligible if precisions of order of a month for AoA are required.

The combined effect of depletion and gravitational separation is seen in the relative difference of "sf6pass" and "sf6" tracers (Fig. 4e and 4f). For both K_z cases the effect of depletion is stronger than the diffusive separation by more than one order of magnitude. Regardless the K_z profiles the reduction exceeds 50 %, which roughly corresponds to 10 years of an offset in the apparent AoA.

In all cases the reduction of the SF_6 content has strong annual cycle associated with the cycle of the downwelling in winter and the upwelling in summer. Besides that the reduction has a noticeable inter-annual variability that poses substantial

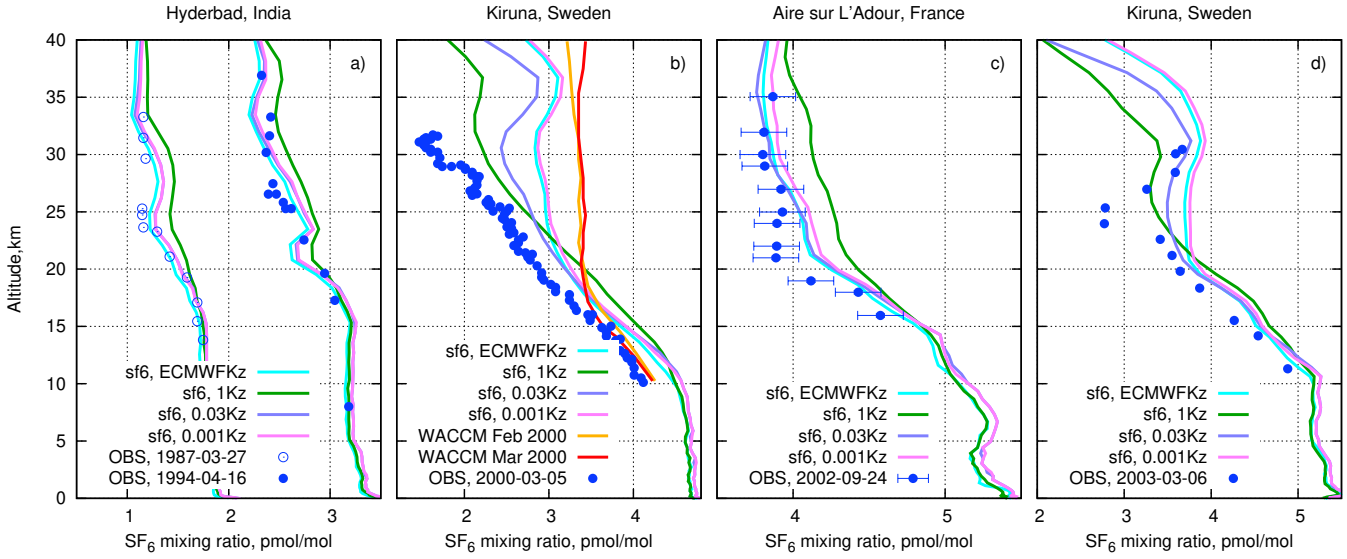

Figure 5. Observed SF_6 balloon profiles and corresponding daily-mean SILAM profiles for the date of observations. The observational data obtained from Patra et al. (1997), Ray et al. (2017), Ray et al. (2014), and Engel et al. (2006) for panels a–d correspondingly. The observation uncertainties are about 2% (1σ) for Hyderabad profiles (a), and smaller than the size of the symbol for Kiruna profiles (b,d). The model profiles from WACCM model are from Ray et al. (2017).

difficulties for applying a consistent correction to the apparent AoA. Contrary to the former two comparisons, strong eddy mixing leads to strong reduction of SF_6 since it intensifies the transport to the depletion layers and thus enhances the depletion rate.

The simulations for different K_z have been initialized with the same state obtained from a separate spin-up simulation with "0.01 Kz", which was scaled to match total burden of SF_6 in 1980. Thus a relaxation of the SF_6 vertical distribution during the first few years of the simulations is clearly seen in Fig. 4. For "1 Kz" case (4f) the gradual increase of the difference between SF_6 and its passive version in the troposphere can be seen as well. The rate of this increase is about 0.5% per 39 years of the simulations. This rate should not be confused with the depletion rate of SF_6 in the atmosphere since the difference is a combined effect of depletion and growth of emission rate, despite the latter is exactly the same for both tracers.

The above comparison indicates that depletion has the stronger effect on the SF_6 mixing ratio in the upper stratosphere than gravitational separation and molecular diffusion. However, the important role of molecular diffusion in the model is that it maintains the upward flux towards the mesosphere in the simulations even if the eddy diffusivity ceases.

Further in this paper only the "sf6pass" and "sf6' tracers will be used.

4.2 Evaluation against balloon profiles

The tropospheric concentrations of SF_6 in our simulations have been insensitive to the SF_6 destruction or to the eddy diffusivity profiles in the stratosphere. The difference in the modelled profiles can however be seen above the tropopause. For comparison we took the simulations with prescribed eddy diffusivity in the stratosphere (1Kz, 0.03Kz, and 0.001Kz, see Sec. 3.1), and with dynamic eddy diffusivity "ECMWF Kz". The simulations were matched with the stratospheric balloon observations (Fig. 5) published by Patra et al. (1997); Engel et al. (2006); Ray et al. (2014, 2017).

Two balloon profiles observed at Hyderbad (17.5N,78.6E) in 1987 and 1994 by Patra et al. (1997) indicate an increase of the SF_6 content during the time between the soundings (Fig. 5a). Both profiles have a clear transition layer from tropopause at ~ 17 km to the undisturbed upper stratosphere above ~ 25 km. The simulated profiles agree quite well with the observed profiles, except for the most diffusive case that gave notably smoother profiles and somewhat overstated SF_6 mixing ratios due to too strong upward transport by diffusion through the tropopause and in the lower stratosphere.

The profile in Fig. 5b has been obtained from Kiruna (68N, 21E) in early spring 2000 during the SAGE III Ozone Loss and Validation Experiment, SOLVE, (Ray et al., 2002) with the Lightweight Airborne Chromatograph (Moore et al., 2003). The profile is affected by the polar vortex and clearly indicates a strong reduction of SF_6 with height with a pronounced local minimum at 32 km. The corresponding SILAM profiles tend to overestimate the SF_6 vmr. The SF_6 profiles for "ECMWF Kz" and "0.001Kz" match each other, since vertical mixing is negligible in both cases. The most diffusive profile "1Kz" has the strongest depletion in the upper part, but the largest deviation from the observations below 20 km. The intermediate-diffusion profile ("0.03Kz") is almost as close to the observations as the non-diffusive profile. Moreover, the "0.03Kz" profile has a minimum at the same altitude as the observed one, albeit the modelled minimum is substantially less deep.

For comparison, Fig. 5b also contains monthly-mean profiles from the WACCM simulations of Ray et al. (2017). The WACCM profiles match very well the observations below 17 km, but turn nearly constant above, thus under-representing the depletion of SF_6 inside the polar vortex. Monthly-mean SILAM profiles (not shown) were much closer to the plotted daily profiles than to the ones of WACCM. However, the WACCM simulations did not include the electron attachment mechanism.

For the mid-latitude profile in Fig. 5c from Aire-sur-l'Adour, France (43.7N,0.3W), all SILAM profiles except for "1Kz" fall within the observational error bars provided together with the data by Ray et al. (2017). Similar to the Kiruna case in Fig. 5b, the SILAM profiles are smoother than the observed ones and are unable to reproduce the sharp transition at 20 km.

Another profile from within the polar vortex (Fig. 5d) was observed at the same Kiruna site as the one in Fig. 5b, but three years later. The observed profile also has a minimum that is much deeper than in the modelled profiles. Similar to the case in Fig. 5b, the "0.03Kz" profile is the only one that has a pronounced minimum at the same altitude as the observed one. The minimum is a result of the spring breakdown of the polar vortex when a regular downdraught ceases, and atmospheric layers decouple from each other. The reduced depth of the modelled minimum is probably caused by insufficient decoupling of the layers in the driving meteorology.

In all above cases, the "1Kz" profile is clearly far too diffusive: in the non-polar cases whereas for the Kiruna cases it overstates the lower part of the profiles and smears out the vertical structure of the profiles further above the tropopause.

The SF_6 profiles simulated with "ECMWF Kz" and "0.001Kz" match each other in all simulations, since vertical mixing is negligible in both cases. The SF_6 resulting from the "0.03Kz" case appears to be the most realistic out of the four considered simulations: they are close to the observed ones and have the local minima at the correct altitudes for both Kiruna profiles.

4.3 Evaluation of SF_6 against MIPAS data

The MIPAS observations provide the richest observational dataset for the stratospheric SF_6 profiles. However, each individual observation has a substantial retrieval noise error, which is noticeably larger than the difference between the observation and any of the SILAM simulations. The largest diversity of the modelled SF_6 profiles was observed in polar regions, therefore below we show the mean profiles for each season in the southern and the northern polar areas. Besides that, we consider statistics of the model performance against MIPAS measurements in the lower and upper stratosphere separately. For simplicity, we do not show the statistics for the "ECMWF Kz" runs, since it is very similar to one for "0.001Kz".

For the comparison, the daily mean model profiles were collocated to the observed ones in space and time, after which an averaging kernel of the corresponding MIPAS profile was applied to the SILAM profile. For the comparison we took only the data points with all of the following criteria met:

- MIPAS visibility flag equals 1
- MIPAS Averaging kernel diagonal elements exceed 0.03
- MIPAS retrieval vertical resolution, i.e. the full-width at the half-maximum of the row of the averaging kernel, is better than $20\,\mathrm{km}$
- MIPAS volume mixing ratio noise error of SF_6 is less than $3\,\mathrm{pmol/mol}$

The mean seasonal profiles of the SF_6 mixing ratio for southern and northern polar regions derived from the MIPAS observations and the SILAM simulations for 2007 are given in Fig. 6. In order to facilitate the comparison of our evaluation with the earlier study of Kovács et al. (2017) we have chosen the same year and same layout of the panels as Fig. 3 there. The main differences between Kovács et al. (2017) and the current evaluation are:

- We used averages of collocated model profiles (bold lines). The non-collocated seasonal- and area-mean model profiles are given as thin dashed lines for comparison.
- we use a newer version of MIPAS SF_6 data with considerably larger values (up to $0.6\,\mathrm{pmol/mol}$) in the upper stratosphere, compared to the version that was used by Kovács et al. (2017).
- The horizontal error bars for the observed data indicate the systematic error component that is fully correlated among the profiles and does not cancel out by averaging, or, in other words, the estimate of a possible bias, as analysed by Stiller et al. (2008). These errors are in the order of 4% (below 30 km) up to 10% (at 60 km). The contribution of the retrieval noise error is essentially negligible due to averaging. The error bars shown by Kovács et al. (2017) are noticeably larger, probably indicating that they are for the individual observed values, rather than the uncertainties of the mean.

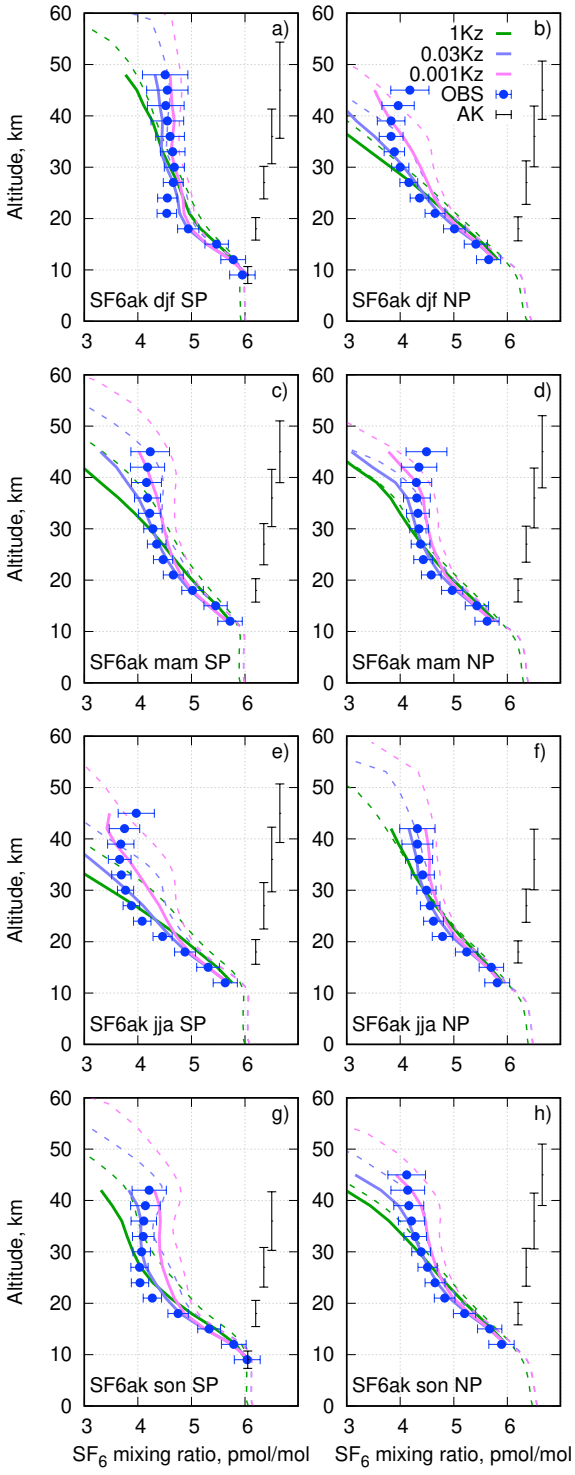

Figure 6. Seasonal mean collocated SILAM SF_6 and MIPAS profiles for 2007, for southern and northern polar regions. Typical ranges covering 75% of the averaging kernel are given with the error bars at the right-hand side of each panel. The horizontal error bars indicate systematic uncertainties of the observations that are fully correlated among profiles and do not cancel out when averaging over a large number of measurements. Dashed lines are zonal-mean SILAM profiles for given season taken without collocation.

– We use 3-km vertical bins for the profiles to make the points in the MIPAS profiles distinguishable

– We also plot the vertical extent of the averaging kernels corresponding to their half-width.

First of all, there is a substantial difference between the collocated and non-collocated model profiles. The difference is caused by the uneven sampling of the atmosphere by the satellite both in space and in time. In particular, MIPAS, being a polar-orbiting instrument, makes more profiles per unit area closer to the pole than further away. The difference gets somewhat reduced if one uses equal weights for all model grid cells instead of area-weighted averaging, especially for wide latitude belts. The major difference comes probably from the inability of MIPAS to retrieve SF_6 profiles in presence of polar stratospheric clouds that clutter lower layers of the stratosphere and make the sampling of polar regions quite uneven both in time and in vertical. This hypothesis agrees with fact that the difference is most pronounced for the winter pole, especially for the south pole in JJA, and almost invisible at a summer pole.

The comparison in Fig. 6 shows that the profiles from the SILAM simulations agree quite well to the observations in the altitude range below 20 – $25\,\mathrm{km}$, with the most diffusive "1Kz" slightly overestimating the SF_6 mixing ratios. In the range above $25\,\mathrm{km}$, the '1Kz" profiles indicate too fast decrease of SF_6 with altitude. The "0.03Kz" profiles give the best results up to $\sim 40\,\mathrm{km}$, except for south pole in JJA and North pole in DJF.

An interesting feature of the winter-pole MIPAS profiles is an increase of the SF_6 mixing ratio above $40\,\mathrm{km}$. This increase might be caused by issues with retrievals as the systematic errors of the retrievals increase with altitude. However, non-monotonic profiles can occur due to the mean atmospheric dynamics (see the non-collocated 0.001Kz profile in Fig. 6g).

None of the model setups is capable of reproducing the observations above 40 km. Wintertime poles also pose a problem to the model. The disagreement indicates a deficiency in the model representation of air flows in the upper part of the domain caused by insufficient vertical resolution of ERA-Interim in the upper stratosphere and lower mesosphere, and a lack of pole-to-pole circulation. This discrepancy is in line with the comparisons in Fig. 5 for polar regions. The model tends to overstate the SF_6 content in the lower part of the polar vortex, and understate it above $40\,\mathrm{km}$.

We also computed statistical scores of the simulated SF_6 mixing ratios for each month of the MIPAS mission. The statistics were computed separately for the altitude range of 10 – $35\,\mathrm{km}$ (Fig. 7) and 30 – $60\,\mathrm{km}$ (Fig. 8). As the difference in the statistical scores between the three selected simulations is quite minor, we used only observations with the retrieval target noise error below $1\,\mathrm{pmol\,mol}^{-1}$.

The root-mean square error turned to be mostly controlled by the bias, and does not allow for clear distinction between the simulated cases. In order to disentangle the effect of bias, we have calculated the standard deviation of the model-measurement difference (STD), absolute bias, and normalised mean bias (NMB):

$$\mathrm{STD(pmol/mol)} = \left\langle \left(M - \langle M\rangle - O + \langle O\rangle\right)^2 \right\rangle^{1/2}, \tag{15}$$

$$\mathrm{Bias(pmol/mol)} = \langle M - O\rangle, \tag{16}$$

$$\mathrm{NMB}(\%) = 2\left\langle \frac{M-O}{M+O} \right\rangle \cdot 100\%, \tag{17}$$

Tracer/ Kz scheme	loss rate, 10^3 mol/year	lifetime, years
passive, any Kz	0	∞
SF_6, ECMWF Kz	440	2900
SF_6, 0.001 Kz	480	2600
SF_6, 0.01 Kz	760	1700
SF_6, 0.03 Kz	800	1540
SF_6, 0.1 Kz	960	1300
SF_6, 1 Kz	2160	590

Table 1. SF_6 destruction rate after stopping the emissions and corresponding lifetimes. Mid-2011 burden of $1.27 \cdot 10^9$ moles is used as a reference for the lifetime estimate

where M and O are modelled and observed values, respectively, and $\langle \cdot \rangle$ denotes averaging over the selected model-observation pairs for the given range of times and altitudes. Along with the STD, we have plotted the RMS error of the observations due to the retrieval noise in the original MIPAS data, labeled as "MIPAS noise" in the top panels of Fig. 7 and Fig. 8.

In the altitude range of 10 – 35 km, the STD of model-measurement difference is uniform in time with minor peaks in August-September (Fig. 7). The level of the noise error constitutes about 85 % of the total model-measurement difference. Application of averaging kernel to the model profiles reduces the STD. The intermediate-diffusivity case "0.03Kz" clearly shows the least STD uniformly over the whole observation period, the same case indicates the least absolute bias.

In the range of 30 – 60 km altitudes (Fig. 8) the level of the retrieval noise is noticeably higher than in the lower stratosphere. The least biased case is "1Kz", which however has the largest STD. The STDs of "0.03Kz" and "0.001Kz" are on par, but the latter has the strongest biase. Thus for this altitude range the intermediate-diffusivity case also shows the best performance.

Note the slight increase of the model bias after 2009, which is likely caused by our overestimating of the emissions rates since that time (see Sec. 3.4). This increase of the bias does not appear in Fig. 8 due to the delay in the response of the content in the upper layers to the changes in surface emissions.

4.4 Lifetime of SF_6 in the atmosphere

In order to estimate the atmospheric lifetime of SF_6 we turned off the emission of all SF_6 tracers in July 2016 and let the model run until the end of 2018 without emissions (Fig. 9). The decrease of the simulated burden after the emission stop can be used to estimate the removal rate from the atmosphere.

Time series of the total burden of SF_6 in the atmosphere in the simulations are given in Fig. 9. For easier comparison to the observed mixing ratios the burden has been normalised with $1.78 \cdot 10^{20}$ moles – the total amount of air in the atmosphere – to get the mean mixing ratio. The tabulated values for the atmospheric burden of SF_6 from Levin et al. (2010) and Rigby et al. (2010) are given for comparison. Since the removal of SF_6 from the atmosphere is mostly controlled by the transport towards the depletion layer, the vertical exchange is the key controlling factor.

The decrease of the atmospheric SF_6 content after the emission stop, is given at the zoom panel of Fig. 9. As expected, after July 2016 the content of passive SF_6 stays constant, while the others begin to decrease at a rate that depends on the transport properties in the stratosphere with the faster removal for the stronger eddy diffusivity. The removal rate is driven by the SF_6 content in the upper stratosphere, which is not in equilibrium with the total atmospheric content. A typical delay between the SF_6 mixing ratio in the troposphere, and the upper stratosphere, i.e. the AoA in the topmost model layer, is about 5-6 years. Therefore, for a reference we used the total amount of atmospheric SF_6 5 years before the emission stop, i.e. $1.23 \times 10^9\,\mathrm{mol}$, which corresponds to the mean mixing ratio of $7\,\mathrm{pmol/mol}$. Dividing the destruction rate with the reference amount one gets the range of corresponding simulated SF_6 life times in the atmosphere: 600 to 2900 years. Despite the range of the tested diffusivities of three orders of magnitude, the loss rate varies only within a factor of five (Table 1).

The term "life time" implies a linear decay, however, due to emissions the distribution of SF_6 in the atmosphere is far from equilibrium, so the decay is not proportional to the burden. A more accurate way to estimate the life time would be to perform a multi-decade simulation without sources, to get the distribution into a quasi-equilibrium with the mesospheric sink. In such quasi-equilibrium the model of linear decay of SF_6 in the whole atmosphere becomes applicable and the life time can be estimated as a simple ratio of the burden to the loss rate. The uncertainty in the equilibrium burden corresponding to the modelled loss rates in Table 1 can be estimated as the range of AoA in the upper stratosphere (~ 0.5 years) divided by the growth rate of the burden ($0.04\,\mathrm{year}^{-1}$), i.e about 2%. A larger uncertainty comes from the over-simplistic parametrization of the loss in the model, which is more difficult to quantify.

The best-performing simulation "0.03Kz" resulted in 1540 years lifetime. Given the uncertainties above, it meets the ranges suggested by earlier studies. It is in a good agreement with the range of 800 – 3200 years from the model studies (Ravishankara et al., 1993; Morris et al., 1995), and is close to the upper bound of the 580–1400 years range recently obtained by (Ray et al., 2017) from the balloon profile given in Fig. 5b.

Our estimate is also slightly above the range given by Kovács et al. (2017), who obtained 1120 – 1475 years. However, in the simulations of Kovács et al. (2017) the mixing ratios of SF_6 in the stratosphere and the lower mesosphere were noticeably higher than those retrieved by MIPAS and practically flat in the range of 30 – 50 km. Such modelled profiles likely indicate too strong vertical exchange in the model, and, as a consequence, too strong loss and corresponding low bias of the estimated lifetime.

5 Simulations of AoA

5.1 Eddy diffusivity and simulated AoA

The effect of the vertical eddy diffusivity on AoA in the stratosphere was evaluated with the same set of three prescribed and one dynamic K_z profiles, as for SF_6 simulations. An example of annual-mean distributions of AoA is given in Fig. 10. The Hunten (1975) K_z profile (Fig. 10a) gives AoA in the stratosphere of about 3.5 years. It is much shorter than the estimates of the stratospheric AoA (e.g. Waugh, 2009; Engel et al., 2009) from the observations of various tracers. Three other profiles of K_z result in almost identical average distributions of AoA with typical stratospheric AoA of 5.5 years, which agrees quite well

with the experimental estimates. In these cases AoA is controlled by the transport with mean winds. Since "0.03Kz" profiles result in most realistic distribution of SF_6 in our simulations, in the current section we will use simulated distributions of tracers with this parameterization.

5.2 AoA and apparent SF_6 AoA

The AoA for all tracers (except for the "ideal age") was calculated as a simple time lag between the mixing ratio at each point of the domain and the mean near-surface mixing ratio. As it has been pointed out by (Waugh and Hall, 2002), this lag equals to AoA only in case of a fully passive tracer with linearly growing (or decreasing) near-surface mixing ratio. Corrections have been applied to the AoA derived from SF_6 in many studies (Volk et al., 1997; Stiller et al., 2008, 2012; Engel et al., 2009) to account for non-linear growth of the near-surface SF_6 mixing ratio and for its mesospheric sink. The corrections rely heavily on various assumptions that can hardly be rigorously verified. Therefore in this study we do not apply any corrections to the AoA derived from the time lags of tracers. The corrections and assumptions behind them are discussed in Sec. 6.

The constant-rate emission of the "passive" tracer resulted in almost linear growth of its near-surface mixing ratio after the spin-up. The latter makes the age derived from the "passive" tracer equivalent to the age derived from the ideal-age tracer. The resulting distributions are indeed very close to each other (Fig. 11 a and b). The agreement confirms the self-consistency of the transport procedure since the tracers have opposite sensitivity to the advection errors: higher mixing ratios correspond to younger air for the accumulating tracers, while for the ideal-age tracer higher mixing ratios correspond to older air. The remaining differences are caused by spatial inhomogeneities of near-surface mixing ratio of "passive"due to variations in the near-surface air density.

The distribution of the AoA derived from "sf6pass" (Fig. 11c) is qualitatively similar to the ideal-age one, however one can see substantial differences. The negative AoA in the northern troposphere for the "sf6pass" tracer is caused by the predominant location of the sources in the northern hemisphere, so the concentrations there exceed the global-mean levels. The growing rate of the SF_6 emissions leads to the faster-than-linear increase of near-surface mixing ratios, which leads to an old bias up to 3-5 months of the "sf6pass" AoA. This old bias has been one of the drawbacks of the SF_6 AoA pointed by Garcia et al. (2011).

The ages shown in Fig. 11a – c agree well with the ages derived from the *in-situ* observations of SF_6 and CO_2 at the 25 km altitude by Waugh and Hall (2002). They also agree quite well with the earlier simulations with five climate models that give annual mean ages in the upper stratosphere between 4.5 and 5.5 years (Butchart et al., 2010). The simulations result in about 1 – 1.5 year younger air than Diabatic mean age obtained with the Lagrangian-model computations of (Diallo et al., 2012) (Fig. 11 is directly comparable with Fig. 2 there) and about 1 year older air than kinematic mean age. Since our pre-processor of wind fields differed strongly from that of Diallo et al. (2012), this similarity is an important indicator of consistency of the numerical procedures applied in both studies.

A substantial disagreement, however, exists with the ages derived from the MIPAS satellite observations (Stiller et al., 2012; Haenel et al., 2015), who calculated ages exceeding 10 years in the polar areas and in the upper stratosphere. The reason for the disagreement follows from the above analysis: SF_6 can neither be considered as a passive tracer nor does its mixing ratio in the troposphere grow linearly with time. Denoting the AoA derived from the SF_6 profiles as "apparent AoA" (Waugh and Hall,

2002), we calculated it from the SILAM-predicted SF_6 profiles, which, as shown above, agree well with AoA derived from MIPAS. The resulting model-based apparent AoA (Fig. 11d) is indeed much older than the "ideal-age" AoA. The distribution of the apparent SF_6 AoA agrees to the AoA retrived from MIPAS SF_6 profiles by Haenel et al. (2015): well over 5 years AoA around equator with well over 10 years AoA in the polar regions.

The effect of the apparent over-aging in the stratosphere due to the subsidence of the mesospheric air was estimated by Stiller et al. (2012) to be a fraction of a year in the upper stratosphere. Earlier experimental balloon studies (Strunk et al., 2000) indicated up to 3.5-year difference between CO_2 and SF_6 ages. In our simulations, the over-aging due to the SF_6 depletion and other factors discussed in the previous sections is much stronger and affects the whole stratosphere.

5.3 Trends in apparent AoA

Changes in the AoA have been used in many studies as an indicator of changes in the atmospheric circulation. In order to evaluate the effect of the way the AoA is computed on its trend we have calculated trends of the apparent AoA at different altitudes and latitudes for 11 years 2002-2012. This period roughly covers the MIPAS mission and allows for comparison with trends reported by Haenel et al. (2015).

The zonal-mean vertical profiles of the AoA trends during 2002-2012 are shown in Fig. 12 for five latitudinal belts. The presented variable is a slope of the linear fit of the deseasonalized monthly-mean time series for each tracer, averaged over the corresponding latitudinal belt and the model layer. The fit was made with the ordinary least-squares method. The error-bars show 95-% confidence intervals calculated as if a model of linear trend with uncorrelated Gaussian noise was applicable to the time series.

The trends of the apparent AoA for the non-passive SF_6 species have a clear increase with height in the upper part of the profiles. Such behaviour agrees well with the AoA trends of Haenel et al. (2015, Fig. 7) obtained from the MIPAS observations. The over-aging due to the mesospheric depletion of SF_6 has been discussed and estimated by Haenel et al. (2015); Kovács et al. (2017). However, Fig. 12 shows that the mesospheric depletion of SF_6 also affects its trend: the over-aging increases with time. The reason is that depletion is proportional to the SF_6 load, which grows with time. This effect has been pointed out and evaluated earlier for N_2O by Schoeberl et al. (2000). For SF_6 the effect of its loss on the AoA was evaluated by Stiller et al. (2012), who concluded that "in-mixing of mesospheric SF_6-depleted air plays a minor role for the assessment of AoA trends", at least within the framework of their approach (2002 – 2010, up to 35 km altitude).

The apparent AoA derived with the passive SF_6 tracer "sf6pass" indicates a negative trend of about 0.5 years/decade. The trend is caused by the temporal variation of SF_6 emissions. In order to get unbiased AoA estimate from the passive tracer, one needs the mixing ratio at the surface increasing linearly with time. A steady growth of emission rate leads to the faster-than-linear increase of the near-surface mixing ratio and, thus, low-bias of the AoA. According to the inventory (Levin et al., 2010) used in this study, the SF_6 emission rate was growing in 1997–2000 about twice slower than after 2005. Consequently, the negative bias of the apparent AoA has increased resulting in the negative trend of the AoA in the stratosphere.

The AoA trends derived from the "ideal age" and "passive" tracers agree through the whole range of altitudes and latitudes indicating internal consistency of our simulations. The main common feature of the profiles is the negative tendency of about

-0.5 year/decade in the altitude range of 15-30 km with a profile that varies across altitudes. Similar-magnitude trends for the same period were reported by Plöger et al. (2015), who used the same ERA-Interim to simulate AoA. The major difference between the obtained trends is that we have consistently negative trends for both hemispheres, whereas Plöger et al. (2015) indicate a positive trend of a fraction of year per decade in the altitude range of 20 – $30\,\mathrm{km}$ in the Northern hemisphere, and a similar-magnitude negative trend in the Southern hemisphere. The reason for the discrepancy deserves further investigation. Possible reason for the discrepancy likely is that Plöger et al. (2015) used diabatic heating rates as vertical velocity, and it is known that the diabatic and kinematic vertical transport is inconsistent in the reanalysis (Abalos et al., 2015).

The trends might be a feature of the non-uniformity of the ERA-Interim dataset, which was produced with assimilation of an inhomogeneous set of the observations. During 2002-2012, the amount of the assimilated data of the upper-air temperatures was by an order of magnitude higher than before 2000 and two orders of magnitude higher than after 2010 (Dee et al., 2011). It had a clear impact on the patterns of the analysis increments in ERA-Interim and, consequently, on the predicted stratospheric circulation. Due to such inhomogeneities, the quality of trends derived from reanalysis data needs to be verified for each geophysical quantity (Dee et al., 2011). Deducing reliable trends for atmospheric temperature, a quantity that is measurable and extensively assimilated, took a major effort (Simmons et al., 2014). The fact that the AoA is not a directly observable quantity makes the verification of the AoA trends difficult.

To get more insight on the nature of the simulated long-term AoA variability at different altitudes and latitudes we have plotted the time series of the monthly zonal-mean ideal-age AoA for the same latitude belts as in Fig. 12 over 1990-2018 (Fig. 13). To make the temporal variations more visible, the mean AoA profile for each latitude averaged over the same period was subtracted from the profiles. One can see a clear seasonal variation of the AoA outside the equatorial zone. The variation has opposite phases in the upper and the lower stratosphere. In the altitude range of 20 – $30\,\mathrm{km}$, where the trends are most pronounced, the temporal variation of the AoA has a ramp structure with more-or-less steady intervals and relatively quick changes. Such structure is similar to the one shown for the ERA-Interim analysis increments (Dee et al., 2011) and is likely to be caused by temporal inhomogeneities in the assimilated dataset. Therefore we do not draw any conclusion here on the actual trends of AoA but highlight that trends of the apparent AoA are strongly influenced by the selected time interval and by the method of the trends calculation.

6 Discussion

The present study has several limitations that deserve specific attention. Forced zero air flux through the domain top at $0.1\,\mathrm{hPa}$ caused distortion of the mean transport within the domain, and left diffusive transport as the only means for the upper-boundary fluxes of $\mathrm{SF_6}$. Secondly, we used prescribed profiles of the eddy diffusivity within the domain, which also affects the results of the simulations. In this section we evaluate the role of these distortions.

6.1 Distortions of air-flows

The transport procedure used in this study is done with a "hardtop" diagnostics forcing zero mass-fluxes at the domain top and forced air-mass conservation everywhere within the domain. Since the upper boundary of the domain is at 0.1 hPa, the divergence of the air flow above that level in the meteorological data used to drive the model is compensated by adjusting the divergences within the domain. To evaluate the effect of this adjustment on the mean circulations we used the new ERA-5 dataset, which has the topmost level at $1 \times 10^{-3}\,\mathrm{hPa}$. The diagnostic procedure was applied to ERA5 for two sets of vertical layers: the 61 ERA-Interim layers, same as used in the SF_6 simulations (hereafter ERA5-cut), and a refined vertical matching the 137 native ERA5 vertical layers (hereafter ERA5). The resulting vertical winds were compared to the ones used in the SF_6 simulations: 61 layers diagnosed from ERA-Interim. The seasonal and zonal-mean vertical air-mass fluxes, expressed in units of Pa/day for the three cases and two solstice seasons of 2017 are shown in Fig. 14 together with the corresponding layer boundaries.

The wind patterns in ERA5 (Fig. 14abde) have finer features than in ERA-Interim due to the higher horizontal resolution. The difference between the ERA5 and ERA5-cut vertical winds is the strongest at the cut-domain top (0.1 hPa, 65 km), where the zero vertical air-mass flux is forced. For both seasons the disturbances introduced by the cut vertical are minor, except for the summertime poles (South pole in Fig. 14ab, and North pole in Fig. 14de), where a noticeable disturbance is visible down to 35-40 km altitude. Such systematic disturbances influence the performance of the AoA and the SF_6 simulations in the polar stratosphere, and they are a probable reason for the failure of the model to reproduce the SF_6 profiles there (see Fig. 6).

The comparison of the mass-fluxes for the same vertical levels (panels b vs. c, or e vs. f in Fig. 14) shows that the difference between ERA-Interim and ERA5 is noticeably larger than between cut- and full vertical of ERA5. Thus we conclude that the distortions introduced by our diagnostic procedure are within the uncertainty of the input meteorological data.

6.2 Top-boundary mass fluxes and eddy diffusion profiles

The used modelling approach replaces the vertical transport through the domain top with the diffusive fluxes for the depleting SF_6 and a hard lid for other species. This approach is unlikely to introduce major disturbances into the AoA fields since the AoA is quite uniform close to the domain top. The uncertainty introduced with this approach into the SF_6 fields is not straightforward to evaluate due to a major uncertainty in the vertical diffusivity profiles.

As mentioned in Sec. 3.1, the eddy diffusivity profiles of the C-IFS model from the ERA5 reanalysis (Fig. 1) are clearly unrealistic within and above the stratosphere. They do not exhibit any growth of the eddy diffusivity in the mesosphere either. According to Lindzen (1981) the mean diffusivity due to the breaking gravity waves has an order of magnitude of $1 \times 10^2\,\mathrm{m}^2/\mathrm{s}$, whereas the eddy diffusion in ERA5 for that region is below the molecular diffusivity (Fig. 1). On the other hand, if we assume that the mesospheric turbulence results in a diffusivity profile as predicted by Lindzen (1981) (Fig. 1) then such turbulence provides quite rapid exchange of SF_6 towards the depletion layers making the advective vertical transport above $\sim 50\,\mathrm{km}$ negligible. The profiles of (Lindzen, 1981), however, do not allow for a simple extrapolation below 50 km and therefore the

vertical profiles by Massie and Hunten (1981) ("1Kz") were involved as the ones that are simple to implement and smooth enough to be easily approximated and extrapolated.

The normalized diffusive SF_6 mass-fluxes above the domain top for the scaled profiles of the eddy diffusivity (Fig. 3) allow for evaluation of the validity of the assumption of neglected regular vertical transport above the domain top. The equivalent vertical air-mass flux due to diffusion at the level of $0.1\,\mathrm{hPa}$ (domain top) is 6×10^{-6}, 9×10^{-7}, and $2.5 \times 10^{-7}\,\mathrm{kg/m^2/s}$ for "1Kz", "0.03Kz", and "0.001Kz" respectively. These mass fluxes, divided by g give the vertical velocities of -5, -0.8, and $-0.4\,\mathrm{Pa/day}$. Comparing these values to those shown in Fig. 14 for the level of 65 km, one can see that the diffusive limit is valid for the "1Kz" profile except for the very vicinities of the poles. For lower values of the eddy diffusivity the regular circulation becomes comparable with the diffusion or even exceed it.

Although the "0.03Kz" profiles gave better agreement with the observations of SF_6, this does not indicate that "0.03Kz" profiles are more realistic. This profile is likely to over-mix the lower stratosphere and under-mix the upper stratosphere and the mesosphere. Thus the vertical structure of the eddy diffusivity remains a major source of uncertainty in the modelling approach. Using more realistic vertical diffusion profiles and high-top ERA5 reanalysis is planned for the future studies.

6.3 Notes on the observed SF_6-age

There are three main factors responsible for the SF_6 age being different from the "ideal age": the non-linear growth of tropospheric burden, the gravitational separation, and the mesospheric sink. Here we consider the effects of these factors and corrections to the SF_6 observations that can be applied to compensate for the effect of these factors on the resulting AoA.

The correction for the non-linear growth rate introduced by Volk et al. (1997) and used in many subsequent studies is based on a simple analytical model of 1D diffusion with constant diffusivity and exponential distribution of air density. The model was suggested by (Hall and Plumb, 1994) as an illustration for the concept of the age spectrum. The model spectrum has two parameters: the mean age Γ and the width parameter Δ. In order to use the spectrum for the correction one has to involve an additional constraint connecting these parameters. Based on a 3D simulation with a general circulation model Hall and Plumb (1994) suggested that a constant ratio $\Delta^2/\Gamma = 0.7\,\mathrm{year}$ can be used throughout the stratosphere. Note that this dimensional parameter, while having proper units originally, appears without units in several subsequent papers (Engel et al., 2002; Stiller et al., 2012). Volk et al. (1997) used the value $\Delta^2/\Gamma = (1.25 \pm 0.50)\,\mathrm{year}$ for the lower stratosphere based on the results of a more advanced GCM than the one used by (Hall and Plumb, 1994). With this approach Volk et al. (1997) obtained the difference between the mean age and the lag time (apparent SF_6 age). The difference becomes significant for the air older than 3-4 years and approaches $(0.50 \pm 0.25)\,\mathrm{years}$ for the oldest (6 years) air, which agrees quite well with the difference between the ideal age and the passive SF_6 in our simulations (Fig. 11bc). The correction for this difference derived from the 1D has been used to reduce the systematic biases from the SF_6-based AoA, though "the global stratosphere is poorly represented by a 1-D model" (Waugh and Hall, 2002). The uncertainty of the correction of up to $\pm 0.5\,\mathrm{years}$ is systematic, is not guaranteed to be uniform in space or in time, and is likely to affect the trend estimates.

As shown in Sec. 4.1, the biases introduced to the SF_6-based AoA by gravitational separation reach a fraction of a year in the upper stratosphere. One could in principle elaborate a correction for gravitational separation; however, the correction would be well within the uncertainty of the correction for the non-linear growth rate, and thus probably not worth considering.

The mesospheric sink has the largest impact on the SF_6-derived AoA. The effect of the mesospheric sink is clearly visible above 15-20 km at all latitudes (Fig. 11) and leads to a strong over-aging in the upper layers, especially in the polar areas. The effect of the sink alone can explain the discrepancy between the AoA derived from the MIPAS observations (Haenel et al., 2015) and the AoA from the modelling studies (e.g. Diallo et al., 2012; Brinkop and Jöckel, 2019). Compensating for such over-aging is hardly possible without detailed modelling of the physical processes including depletion, diffusion and mean transport. Since the AoA is derived as a *difference* of the SF_6 mixing ratios, whereas depletion introduces *multiplicative* change to the SF_6 abundance, the effect of the sink on apparent SF_6 AoA is unsteady in time (Fig. 12).

Once one has a model that is capable of reproducing the processes behind the SF_6 depletion, it is natural to validate such a model directly against the available SF_6 observations, rather than deriving the AoA from the SF_6 observations and comparing it against the modelled one. In any case the AoA derived from the SF_6 tracer observations with all the corrections cannot be considered as a purely observed one.

7 Conclusions

Eulerian simulations of the tropospheric and stratospheric transport of several tracers were performed with the SILAM model driven by the ERA-Interim reanalysis for 1980-2018. The simulations included species representing SF_6 under different assumptions, a passive tracer emitted uniformly at the surface, and an "ideal age" tracer directly comparable to other state-of-the-art CTM simulations of the AoA. To our best knowledge this is the first systematic evaluation of AoA derived from several different tracers within the same multi-decadal simulation, combined with the extensive evaluation against MIPAS and balloon SF_6 observations.

Due to the limited vertical coverage and resolution of ERA-Interim in the upper stratosphere, the SILAM simulation domain had a lid at $0.1\,\mathrm{hPa}$, which is below the altitude of the SF_6 destruction. In order to perform realistic simulations of SF_6 in our setup, the eddy diffusion in the upper stratosphere and lower mesosphere had to be parameterised, along with the mesospheric sink of SF_6.

A set of simulations with different parameterisations for the vertical eddy diffusion showed that published profiles derived with no account for advection (see e.g. Massie and Hunten, 1981, and references threrin) overestimate the eddy diffusivity. On other hand, the eddy-diffusivity profiles for scalars calculated from the ERA-Interim fields according to the IFS procedures ECMWF (2015)), or readily available from the ERA5 reanalysis, appear to be of no relevance for the upper stratosphere, since they fall below the molecular diffusivity. Evaluation of our simulations against satellite and balloon observations indicated that the best agreement between the simulated and observed SF_6 mixing ratios within the model domain is achieved for the tabulated eddy-diffusivity profile of Hunten (1975) scaled down with a factor of 30. However, this conclusion is likely to be

a feature the specific model setup. Thus, the question of the importance and magnitude of the eddy diffusivity in the upper stratosphere and lower mesosphere remains open and the SF_6 observations are potentially a good means of its evaluation.

The mesospheric sink of SF_6 has a major impact on the mixing ratios above $20\,km$. The depletion impact is especially strong in the wintertime polar areas due to the descent within a polar vortex. A set of sensitivity tests showed that molecular diffusion and gravitational separation of SF_6 are responsible for up to a few percent of further reduction in SF_6 mixing ratios in the upper stratosphere.

A good agreement of the simulated SF_6 distribution with the MIPAS observations up to the altitudes of 30-35 km and with the available balloon profiles was shown. The standard deviation between the MIPAS and the modelled SF_6 mixing ratios is mainly 80 % controlled by the noise error of the satellite retrievals, i.e. the standard deviation between model and MIPAS is about as large as the error on the satellite data. The results of the comparison also underline the importance of accurate collocation of the modeled and the observed data in terms of space, time and vertical averaging of the observed data.

The lifetime of SF_6 in the atmosphere estimated from the best-performing setup is about 1500 years, which is at the high side of the range of other recent estimates. Our estimate is likely to be biased high due to underrepresented vertical exchange to at the domain top due to missing advective transport and the missing effect of breaking gravity waves.

Our simulations were able to reproduce both AoA obtained in other model studies, and the apparent SF_6 AoA derived from the MIPAS observations. This highlights the role of fast mesospheric destruction of SF_6 due to the electron attachment mechanism. Having all tracers within the same simulations we were able to trace the differences in the estimated AoA to the peculiarities of each tracer. A good agreement of the passive-tracer and "ideal-age" AoA indicates a consistency of the simulations, since these two methods have opposite sign of sensitivity to errors of the transport scheme.

The mesospheric sink has severe implications on the AoA derived from the SF_6. The apparent over-aging introduced by the sink is large and variable in space and time. Moreover, the over-aging due to the sink increases as the atmospheric burden of SF_6 grows. All this makes SF_6 unsuitable to infer AoA above $\sim 20\,km$. For a fully-passive SF_6 tracer, the variable rate of emissions causes deviations from the "ideal age", and these deviations can be compensated to some extent. However, correcting the deviations due to the mesospheric sink of SF_6 is hardly possible. These deviations appear as long-term trends in the apparent AoA. These trends differ from the trends in the "ideal-age AoA", and have no direct correspondence to the actual trends in the atmospheric circulation.

Procedures used to derive the AoA from observations of various tracers in the atmosphere are inevitably based on assumptions and idealisations that have limited and often unknown area of applicability. The resulting uncertainties in the AoA are large enough to preclude the use of apparent AoA and its trends for evaluation of changes in atmospheric circulation or for validation of atmospheric models. Observations of the tracers themselves, however, have well quantified uncertainties, so direct comparisons of simulated tracers to the observed ones are a very promising means for the atmospheric model evaluation. AoA in turn is a convenient means for model inter-comparison if a protocol of the AoA derivation is well specified.

Code and data availability. The SILAM source code is freely available from GitHub (https://github.com/fmidev/silam-model). The simulation results are available from MS or RK on request. The MIPAS observational data available from GS on request. ERA-Interim and ERA5 reanalyses data sets are available from the European Center for Medium-range weather forecast http://www.ecmwf.int.

Author contributions. RK performed the simulations and data analyses, prepared text and illustrations. MS and JV inspired the study and helped with discussions on content and structure of the study, and participated in editing the text. GS provided MIPAS data and wrote sections about MIPAS observations. All authors participated in the final preparation of the text.

Competing interests. The authors declare no competing interests.

Acknowledgements. The authors acknowledge the support of projects: EU FP7-MarcoPolo (ID: 606953), ESA-ATILA (contract no. 4000105828/12/F/MO and ASTREX of Academy of Finland (grant 139126), Russian Foundation for Basic Research (project 19-05-01008).

The SF_6 and mean age-of-air distributions from MIPAS observations were generated within the project STI 210/5-3 of the CAWSES priority program, funded by the German Research Foundation (DFG), and the project BDCHANGE (01LG1221B), funded by the German Federal Ministry of Education and Research (BMBF) within the "ROMIC" program.

The authors are grateful to Viktoria Sofieva (Finnish Meteorological institute) for reading the manuscript and providing useful comments, to Florian Haenel and Michael Kiefer (Karlsruhe Institute of Technology) for technical assistance in handling MIPAS SF_6 data, and to four anonymous reviewers whose very instrumental comments helped to substantially improve the paper.

References

Abalos, M., Legras, B., Ploeger, F., and Randel, W. J.: Evaluating the advective Brewer-Dobson circulation in three reanalyses for the period 1979–2012, Journal of Geophysical Research: Atmospheres, 120, 7534–7554, https://doi.org/10.1002/2015JD023182, 2015.

Allen, M., Yung, Y. L., and Waters, J. W.: Vertical transport and photochemistry in the terrestrial mesosphere and lower thermosphere (50–120 km), J. Geophys. Res., 86, 3617–3627, https://doi.org/10.1029/JA086iA05p03617, 1981.

Andrews, A. E., Boering, K. A., Daube, B. C., Wofsy, S. C., Loewenstein, M., Jost, H., Podolske, J. R., Webster, C. R., Herman, R. L., Scott, D. C., and et al.: Mean ages of stratospheric air derived from in situ observations of CO2, CH4, and N2O, J. Geophys. Res., 106, 32 295–32 314, https://doi.org/10.1029/2001jd000465, 2001.

Bhandari, N., Lal, D., and Rama, D.: Stratospheric circulation studies based on natural and artificial radioactive tracer elements, Tellus, 18, 391–406, https://doi.org/10.1111/j.2153-3490.1966.tb00250.x, 1966.

Boering, K., Wofsy, S., Daube, B., Schneider, H., Loewenstein, M., Podolske, J., and Conway, T.: Stratospheric mean ages and transport rates from observations of carbon dioxide and nitrous oxide, Science, 274, 1340–1343, https://doi.org/10.1126/science.274.5291.1340, 1996.

Brinkop, S. and Jöckel, P.: ATTILA 4.0: Lagrangian advective and convective transport of passive tracers within the ECHAM5/MESSy chemistry–climate model, Geoscientific Model Development, 12, 1991–2008, 2019.

Butchart, N., Cionni, I., Eyring, V., Shepherd, T. G., Waugh, D. W., Akiyoshi, H., Austin, J., Brühl, C., Chipperfield, M. P., Cordero, E., and et al.: Chemistry–Climate Model Simulations of Twenty-First Century Stratospheric Climate and Circulation Changes, J. Climate, 23, 5349–5374, https://doi.org/10.1175/2010jcli3404.1, 2010.

Copernicus Climate Change Service (C3S): ERA5: Fifth generation of ECMWF atmospheric reanalyses of the global climate, Copernicus Climate Change Service Climate Data Store (CDS), 2018, https://cds.climate.copernicus.eu/cdsapp#!/home, 2017.

Cussler, E. L.: Diffusion: Mass Transfer in Fluid Systems (Cambridge Series in Chemical Engineering), Cambridge University Press, 1997.

Dee, D. P., Uppala, S. M., Simmons, A. J., Berrisford, P., Poli, P., Kobayashi, S., Andrae, U., Balmaseda, M. A., Balsamo, G., Bauer, P., and et al.: The ERA-Interim reanalysis: configuration and performance of the data assimilation system, Q. J. Roy. Meteorol. Soc., 137, 553–597, https://doi.org/10.1002/qj.828, 2011.

Diallo, M., Legras, B., and Chédin, A.: Age of stratospheric air in the ERA-Interim, Atmos. Chem. Phys., 12, 12 133–12 154, https://doi.org/10.5194/acp-12-12133-2012, 2012.

ECMWF: IFS Documentation – Cy41r1, Part 4: Physical processes, Tech. rep., European Center for Medium-range Weather Forecasts, http://old.ecmwf.int/publications/library/do/references/list/151, 2015.

Eluszkiewicz, J., Hemler, R. S., Mahlman, J. D., Bruhwiler, L., and Takacs, L. L.: Sensitivity of Age-of-Air Calculations to the Choice of Advection Scheme, J. Atmos. Sci., 57, 3185–3201, https://doi.org/10.1175/1520-0469(2000)057<3185:SOAOAC>2.0.CO;2, 2000.

Engel, A., Strunk, M., Müller, M., Haase, H.-P., Poss, C., Levin, I., and Schmidt, U.: Temporal development of total chlorine in the high-latitude stratosphere based on reference distributions of mean age derived from CO2 and SF6, Journal of Geophysical Research: Atmospheres, 107, ACH–1, 2002.

Engel, A., Möbius, T., Haase, H.-P., Bönisch, H., Wetter, T., Schmidt, U., Levin, I., Reddmann, T., Oelhaf, H., Wetzel, G., et al.: Observation of mesospheric air inside the arctic stratospheric polar vortex in early 2003, Atmospheric Chemistry and Physics, 6, 267–282, https://doi.org/1680-7324/acp/2006-6-267, 2006.

Engel, A., Möbius, T., Bönisch, H., Schmidt, U., Heinz, R., Levin, I., Atlas, E., Aoki, S., Nakazawa, T., Sugawara, S., and et al.: Age of stratospheric air unchanged within uncertainties over the past 30 years, Nature Geosci, 2, 28–31, https://doi.org/10.1038/ngeo388, 2009.

Engel, A., Rigby, M., Burkholder, J., Fernandez, R., Froidevaux, L., Hall, B., Hossaini, R., Saito, T., Vollmer, M., and Yao, B.: Update on Ozone-Depleting Substances (ODSs) and Other Gases of Interest to the Montreal Protocol, Chapter 1 in Scientific Assessment of Ozone Depletion: 2018, Report 58, World Meteorological Organization, Geneva, Switzerland, https://www.esrl.noaa.gov/csd/assessments/ozone/2018/, 2018.

England, M. H.: The age of water and ventilation timescales in a global ocean model, Journal of Physical Oceanography, 25, 2756–2777, https://doi.org/10.1175/1520-0485(1995)025<2756:TAOWAV>2.0.CO;2, 1995.

Garcia, R. R., Randel, W. J., and Kinnison, D. E.: On the determination of age of air trends from atmospheric trace species, Journal of the Atmospheric Sciences, 68, 139–154, https://doi.org/10.1175/2010JAS3527.1, 2011.

Garny, H., Birner, T., Bönisch, H., and Bunzel, F.: The effects of mixing on age of air, Journal of Geophysical Research: Atmospheres, 119, 7015–7034, 2014.

Gavrilov, N. M., Luce, H., Crochet, M., Dalaudier, F., and Fukao, S.: Turbulence parameter estimations from high-resolution balloon temperature measurements of the MUTSI-2000 campaign, Annales Geophysicae, 23, 2401–2413, https://doi.org/10.5194/angeo-23-2401-2005, 2005.

Haenel, F. J., Stiller, G. P., von Clarmann, T., Funke, B., Eckert, E., Glatthor, N., Grabowski, U., Kellmann, S., Kiefer, M., Linden, A., and Reddmann, T.: Reassessment of MIPAS age of air trends and variability, Atmospheric Chemistry and Physics Discussions, 15, 14 685–14 732, https://doi.org/10.5194/acpd-15-14685-2015, 2015.

Hall, T. M. and Plumb, R. A.: Age as a diagnostic of stratospheric transport, J. Geophys. Res., 99, 1059–1070, https://doi.org/10.1029/93JD03192, 1994.

Hall, T. M., Waugh, D. W., Boering, K. A., and Plumb, R. A.: Evaluation of transport in stratospheric models, Journal of Geophysical Research: Atmospheres, 104, 18 815–18 839, 1999.

Harrison, J. J.: New and improved infrared absorption cross sections for trichlorofluoromethane (CFC-11), Atmospheric Measurement Techniques, 11, 5827–5836, https://doi.org/10.5194/amt-11-5827-2018, 2018.

Heimann, M. and Keeling, C. D.: A three-dimensional model of atmospheric CO2 transport based on observed winds: 2. Model description and simulated tracer experiments, pp. 237–275, American Geophysical Union (AGU), https://doi.org/10.1029/GM055p0237, 1989.

Hunten, D. M.: Estimates of Stratospheric Pollution by an Analytic Model, Proceedings of the National Academy of Sciences of the United States of America, 72, 4711–4715, http://www.jstor.org/stable/65270, 1975.

IPCC: Climate Change 2013: The Physical Science Basis. Contribution of Working Group I to the Fifth Assessment Report of the Intergovernmental Panel on Climate Change, Cambridge University Press, Cambridge, United Kingdom and New York, NY, USA, https://doi.org/10.1017/CBO9781107415324, www.climatechange2013.org, 2013.

Ishidoya, S., Sugawara, S., Morimoto, S., Aoki, S., and Nakazawa, T.: Gravitational separation of major atmospheric components of nitrogen and oxygen in the stratosphere, Geophysical Research Letters, 35, https://doi.org/10.1029/2007gl030456, 2008.

Ishidoya, S., Sugawara, S., Morimoto, S., Aoki, S., Nakazawa, T., Honda, H., and Murayama, S.: Gravitational separation in the stratosphere–a new indicator of atmospheric circulation, Atmospheric Chemistry and Physics, 13, 8787–8796, 2013.

Jacob, D. J., Prather, M. J., Rasch, P. J., Shia, R.-L., Balkanski, Y. J., Beagley, S. R., Bergmann, D. J., Blackshear, W. T., Brown, M., Chiba, M., Chipperfield, M. P., de Grandpré, J., Dignon, J. E., Feichter, J., Genthon, C., Grose, W. L., Kasibhatla, P. S., Köhler, I., Kritz, M. A., Law, K., Penner, J. E., Ramonet, M., Reeves, C. E., Rotman, D. A., Stockwell, D. Z., Van Velthoven, P. F. J., Verver, G., Wild, O., Yang, H., and Zimmermann, P.: Evaluation and intercomparison of global atmospheric transport models using 222Rn and other short-lived tracers, Journal of Geophysical Research: Atmospheres, 102, 5953–5970, https://doi.org/10.1029/96JD02955, 1997.

Koch, D. and Rind, D.: Beryllium 10/beryllium 7 as a tracer of stratospheric transport, Journal of Geophysical Research: Atmospheres, 103, 3907–3917, https://doi.org/10.1029/97JD03117, 1998.

Kovács, T., Feng, W., Totterdill, A., Plane, J. M. C., Dhomse, S., Gómez-Martín, J. C., Stiller, G. P., Haenel, F. J., Smith, C., Forster, P. M., García, R. R., Marsh, D. R., and Chipperfield, M. P.: Determination of the atmospheric lifetime and global warming potential of sulfur hexafluoride using a three-dimensional model, Atmospheric Chemistry and Physics, 17, 883–898, https://doi.org/10.5194/acp-17-883-2017, 2017.

Krol, M., de Bruine, M., Killaars, L., Ouwersloot, H., Pozzer, A., Yin, Y., Chevallier, F., Bousquet, P., Patra, P., Belikov, D., Maksyutov, S., Dhomse, S., Feng, W., and Chipperfield, M. P.: Age of air as a diagnostic for transport timescales in global models, Geoosci. Model Devel., 11, 3109–3130, https://doi.org/10.5194/gmd-11-3109-2018, 2018.

Leedham Elvidge, E., Bönisch, H., Brenninkmeijer, C. A., Engel, A., Fraser, P. J., Gallacher, E., Langenfelds, R., Mühle, J., Oram, D. E., Ray, E. A., et al.: Evaluation of stratospheric age of air from CF_4, C_2F_6, C_3F_8, CHF_3, HFC-125, HFC-227ea and SF_6; implications for the calculations of halocarbon lifetimes, fractional release factors and ozone depletion potentials, Atmospheric Chemistry and Physics, 18, 3369–3385, https://doi.org/10.5194/acp-18-3369-2018, 2018.

Legras, B., Pisso, I., Berthet, G., and Lefèvre, F.: Variability of the Lagrangian turbulent diffusion in the lower stratosphere, Atmos. Chem. Phys., 5, 1605–1622, https://doi.org/10.5194/acp-5-1605-2005, 2005.

Levin, I., Naegler, T., Heinz, R., Osusko, D., Cuevas, E., Engel, A., Ilmberger, J., Langenfelds, R. L., Neininger, B., Rohden, C. v., et al.: The global SF6 source inferred from long-term high precision atmospheric measurements and its comparison with emission inventories, Atmospheric Chemistry and Physics, 10, 2655–2662, https://doi.org/10.5194/acp-10-2655-2010, 2010.

Li, S. and Waugh, D. W.: Sensitivity of mean age and long-lived tracers to transport parameters in a two-dimensional model, Journal of Geophysical Research: Atmospheres, 104, 30 559–30 569, https://doi.org/10.1029/1999JD900913, 1999.

Lindzen, R. S.: Turbulence and stress owing to gravity wave and tidal breakdown, Journal of Geophysical Research: Oceans, 86, 9707–9714, https://doi.org/10.1029/JC086iC10p09707, 1981.

Mange, P.: The theory of molecular diffusion in the atmosphere, Journal of Geophysical Research, 62, 279–296, 1957.

Marrero, T. R. and Mason, E. A.: Gaseous diffusion coefficients, Journal of Physical and Chemical Reference Data, 1, 3–118, https://doi.org/10.1063/1.3253094, 1972.

Massie, S. T. and Hunten, D. M.: Stratospheric eddy diffusion coefficients from tracer data, J. Geophys. Res., 86, 9859–9867, https://doi.org/10.1029/jc086ic10p09859, 1981.

Monge-Sanz, B. M., Chipperfield, M. P., Dee, D. P., Simmons, A. J., and Uppala, S. M.: Improvements in the stratospheric transport achieved by a chemistry transport model with ECMWF (re)analyses: identifying effects and remaining challenges, Q. J. Roy. Meteorol. Soc., 139, 654–673, https://doi.org/10.1002/qj.1996, 2012.

Moore, F., Elkins, J., Ray, E., Dutton, G., Dunn, R., Fahey, D., McLaughlin, R., Thompson, T., Romashkin, P., Hurst, D., et al.: Balloonborne in situ gas chromatograph for measurements in the troposphere and stratosphere, Journal of Geophysical Research: Atmospheres, 108, https://doi.org/1029/2001JD000961, 2003.

Morris, R. A., Miller, T. M., Viggiano, A., Paulson, J. F., Solomon, S., and Reid, G.: Effects of electron and ion reactions on atmospheric lifetimes of fully fluorinated compounds, Journal of Geophysical Research: Atmospheres, 100, 1287–1294, 1995.

NOAA, NASA, and USAF: U.S. Standard Atmosphere, U.S. Governement Printing Office, Washington D.C., 1976.

Osman, M., Hocking, W., and Tarasick, D.: Parameterization of large-scale turbulent diffusion in the presence of both well-mixed and weakly mixed patchy layers, Journal of Atmospheric and Solar-Terrestrial Physics, 143-144, 14–36, https://doi.org/10.1016/j.jastp.2016.02.025, 2016.

Patra, P. K., Lal, S., Subbaraya, B., Jackman, C. H., and Rajaratnam, P.: Observed vertical profile of sulphur hexafluoride (SF6) and its atmospheric applications, Journal of Geophysical Research: Atmospheres, 102, 8855–8859, https://doi.org/10.1029/96JD03503, 1997.

Patra, P. K., Houweling, S., Krol, M., Bousquet, P., Belikov, D., Bergmann, D., Bian, H., Cameron-Smith, P., Chipperfield, M. P., Corbin, K., et al.: TransCom model simulations of CH 4 and related species: linking transport, surface flux and chemical loss with CH 4 variability in the troposphere and lower stratosphere, Atmospheric Chemistry and Physics, 11, 12 813–12 837, https://doi.org/10.5194/acp-11-12813-2011, 2011.

Pisso, I. and Legras, B.: Turbulent vertical diffusivity in the sub-tropical stratosphere, Atmos. Chem. Phys., 8, 697–707, https://doi.org/10.5194/acp-8-697-2008, 2008.

Plöger, F., Abalos, M., Birner, T., Konopka, P., Legras, B., Müller, R., and Riese, M.: Quantifying the effects of mixing and residual circulation on trends of stratospheric mean age of air, Geophysical Research Letters, 42, 2047–2054, https://doi.org/10.1002/2014GL062927, 2015.

Ravishankara, A., Solomon, S., Turnipseed, A., and Warren, R.: Atmospheric lifetimes of long-lived halogenated species, Science, 259, 194–199, 1993.

Ray, E. A., Moore, F. L., Elkins, J. W., Hurst, D. F., Romashkin, P. A., Dutton, G. S., and Fahey, D. W.: Descent and mixing in the 1999–2000 northern polar vortex inferred from in situ tracer measurements, Journal of Geophysical Research: Atmospheres, 107, https://doi.org/10.1029/2001JD000961, 2002.

Ray, E. A., Moore, F. L., Rosenlof, K. H., Davis, S. M., Sweeney, C., Tans, P., Wang, T., Elkins, J. W., Bönisch, H., Engel, A., et al.: Improving stratospheric transport trend analysis based on SF6 and CO2 measurements, Journal of Geophysical Research: Atmospheres, 119, 14–110, https://doi.org/10.1002/2014JD021802, 2014.

Ray, E. A., Moore, F. L., Elkins, J. W., Rosenlof, K. H., Laube, J. C., Röckmann, T., Marsh, D. R., and Andrews, A. E.: Quantification of the SF6 lifetime based on mesospheric loss measured in the stratospheric polar vortex, Journal of Geophysical Research: Atmospheres, 122, 4626–4638, https://doi.org/10.1002/2016JD026198, 2017.

Reddmann, T., Ruhnke, R., and Kouker, W.: Three-dimensional model simulations of SF6 with mesospheric chemistry, Journal of Geophysical Research: Atmospheres, 106, 14 525–14 537, https://doi.org/10.1029/2000JD900700, 2001.

Remsberg, E. E.: Methane as a diagnostic tracer of changes in the Brewer-Dobson circulation of the stratosphere, Atmos. Chem. Phys., 15, 3739–3754, https://doi.org/10.5194/acp-15-3739-2015, 2015.

Rigby, M., Mühle, J., Miller, B. R., Prinn, R. G., Krummel, P. B., Steele, L. P., Fraser, P. J., Salameh, P. K., Harth, C. M., Weiss, R. F., and et al.: History of atmospheric SF6 from 1973 to 2008, Atmos. Chem. Phys., 10, 10 305–10 320, https://doi.org/10.5194/acp-10-10305-2010, 2010.

Schoeberl, M. R., Sparling, L. C., Jackman, C. H., and Fleming, E. L.: A Lagrangian view of stratospheric trace gas distributions, Journal of Geophysical Research: Atmospheres, 105, 1537–1552, https://doi.org/10.1029/1999JD900787, 2000.

Simmons, A., Poli, P., Dee, D., Berrisford, P., Hersbach, H., Kobayashi, S., and Peubey, C.: Estimating low-frequency variability and trends in atmospheric temperature using ERA-Interim, Quarterly Journal of the Royal Meteorological Society, 140, 329–353, https://doi.org/10.1002/qj.2317, 2014.

Smith, A. K., Garcia, R. R., Marsh, D. R., and Richter, J. H.: WACCM simulations of the mean circulation and trace species transport in the winter mesosphere, Journal of Geophysical Research: Atmospheres, 116, https://doi.org/10.1029/2011JD016083, 2011.

Sofiev, M., Vira, J., Kouznetsov, R., Prank, M., Soares, J., and Genikhovich, E.: Construction of the SILAM Eulerian atmospheric dispersion model based on the advection algorithm of Michael Galperin, Geoosci. Model Devel., 8, 3497–3522, https://doi.org/10.5194/gmd-8-3497-2015, 2015.

Stiller, G. P., von Clarmann, T., Höpfner, M., Glatthor, N., Grabowski, U., Kellmann, S., Kleinert, A., Linden, A., Milz, M., Reddmann, T., Steck, T., Fischer, H., Funke, B., López-Puertas, M., and Engel, A.: Global distribution of mean age of stratospheric air from MIPAS SF_6 measurements, Atmos. Chem. Phys., 8, 677–695, https://doi.org/10.5194/acp-8-677-2008, 2008.

Stiller, G. P., von Clarmann, T., Haenel, F., Funke, B., Glatthor, N., Grabowski, U., Kellmann, S., Kiefer, M., Linden, A., Lossow, S., and Lopez-Puertas, M.: Observed temporal evolution of global mean age of stratospheric air for the 2002 to 2010 period, Atmos. Chem. Phys., 12, 3311–3331, https://doi.org/10.5194/acp-12-3311-2012, 2012.

Strunk, M., Engel, A., Schmidt, U., Volk, C. M., Wetter, T., Levin, I., and Glatzel-Mattheier, H.: CO2 and SF6 as stratospheric age tracers: Consistency and the effect of mesospheric SF6-loss, Geophysical Research Letters, 27, 341–344, https://doi.org/10.1029/1999GL011044, 2000.

Sugawara, S., Ishidoya, S., Aoki, S., Morimoto, S., Nakazawa, T., Toyoda, S., Inai, Y., Hasebe, F., Ikeda, C., Honda, H., et al.: Age and gravitational separation of the stratospheric air over Indonesia, Atmospheric Chemistry and Physics, 18, 1819–1833, 2018.

Thiele, G. and Sarmiento, J. L.: Tracer dating and ocean ventilation, Journal of Geophysical Research: Oceans, 95, 9377–9391, https://doi.org/10.1029/JC095iC06p09377, 1990.

Totterdill, A., Kovács, T., Gómez Martín, J. C., Feng, W., and Plane, J. M. C.: Mesospheric Removal of Very Long-Lived Greenhouse Gases SF6 and CFC-115 by Metal Reactions, Lyman-α Photolysis, and Electron Attachment, The Journal of Physical Chemistry A, 119, 2016–2025, https://doi.org/10.1021/jp5123344, 2015.

Varanasi, P., Li, Z., Nemtchinov, V., and Cherukuri, A.: Spectral absorption-coefficient data on HCFC-22 and SF_6 for remote-sensing applications, Journal of Quantitative Spectroscopy and Radiative Transfer, 52, 323–332, https://doi.org/10.1016/0022-4073(94)90162-7, 1994.

Volk, C. M., Elkins, J. W., Fahey, D. W., Dutton, G. S., Gilligan, J. M., Loewenstein, M., Podolske, J. R., Chan, K. R., and Gunson, M. R.: Evaluation of source gas lifetimes from stratospheric observations, Journal of Geophysical Research: Atmospheres, 102, 25 543–25 564, https://doi.org/10.1029/97JD02215, 1997.

Waugh, D.: Atmospheric dynamics: The age of stratospheric air, Nature Geosci, 2, 14–16, https://doi.org/10.1038/ngeo397, 2009.

Waugh, D. W. and Hall, T. M.: Age of stratospheric air: Theory, observations, and models, Reviews of Geophysics, 40, https://doi.org/10.1029/2000rg000101, 2002.

Waugh, D. W., Hall, T. M., and Haine, T. W. N.: Relationships among tracer ages, Journal of Geophysical Research: Oceans, 108, 3138, https://doi.org/10.1029/2002JC001325, 2003.

Wilson, R.: Turbulent diffusivity in the free atmosphere inferred from MST radar measurements: a review, Annales Gephysicae, 22, 3869–3887, https://doi.org/10.5194/angeo-22-3869-2004, 2004.

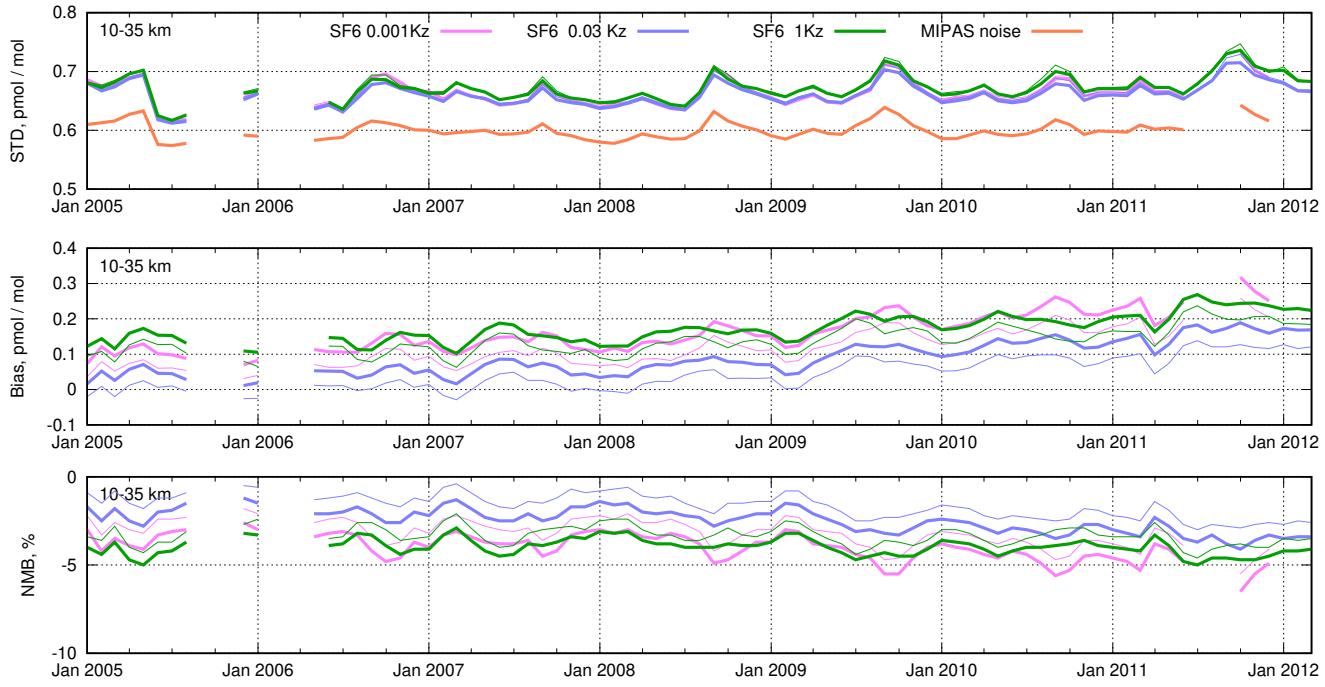

Figure 7. Time series of monthly scores for the SILAM SF_6 mixing ratios for the whole period of the MIPAS observations in the altitude range of $10 - 35\,\mathrm{km}$. The statistics are standard deviation of model-measurement difference (STD), absolute bias and normalised mean bias (NMB). The statistics of the model mixing ratios extracted at nominal MIPAS altitudes are given as thin lines.

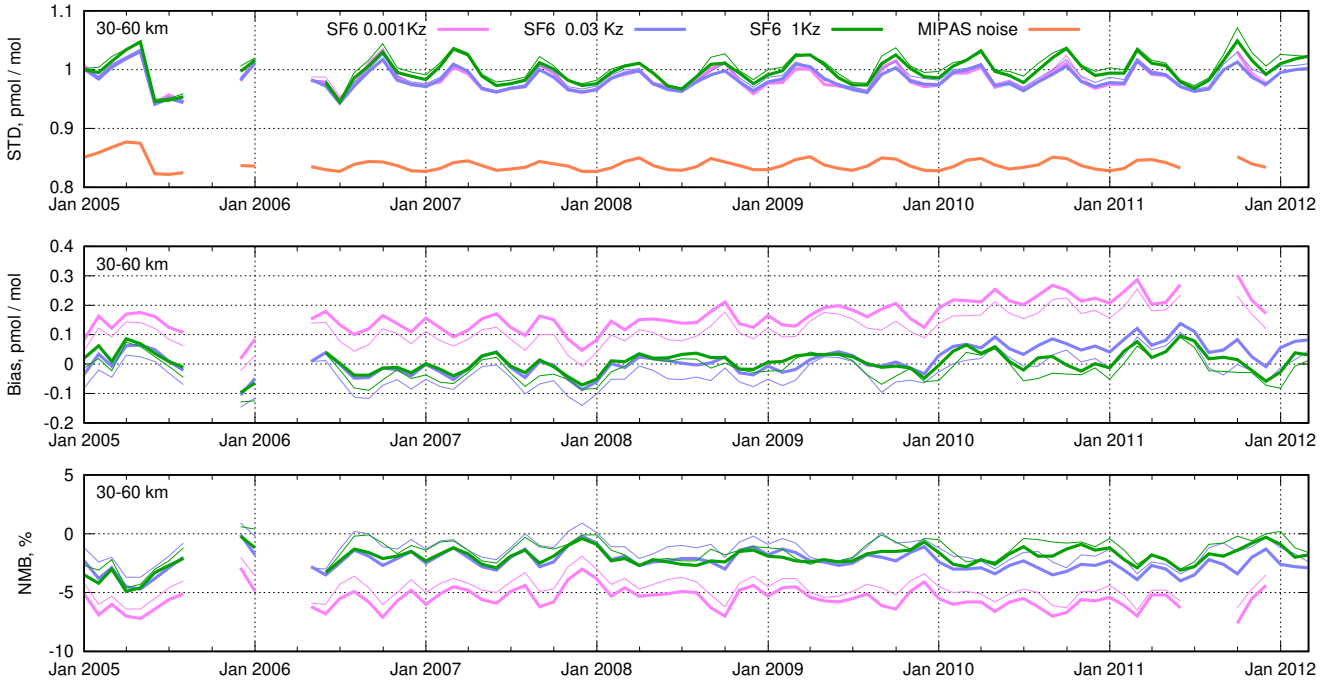

Figure 8. Same as in Fig. 7, but for the MIPAS altitude range of $30 - 60\,\mathrm{km}$.

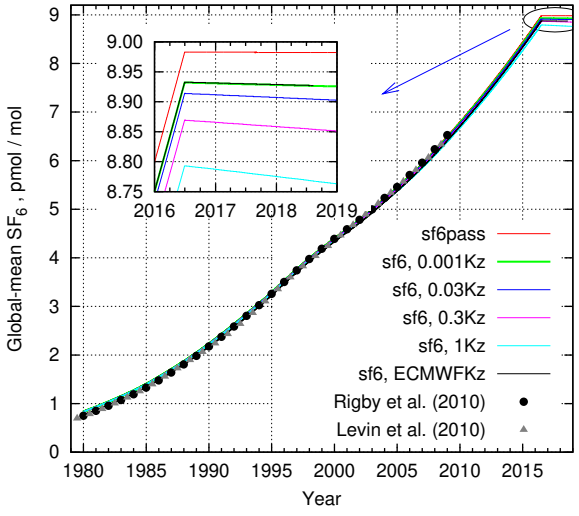

Figure 9. The time series of mean mixing ratio of SF_6 in the atmosphere simulated with emissions stopped in July 2016. The total burdens by Levin et al. (2010) and by Rigby et al. (2010) are shown for comparison.

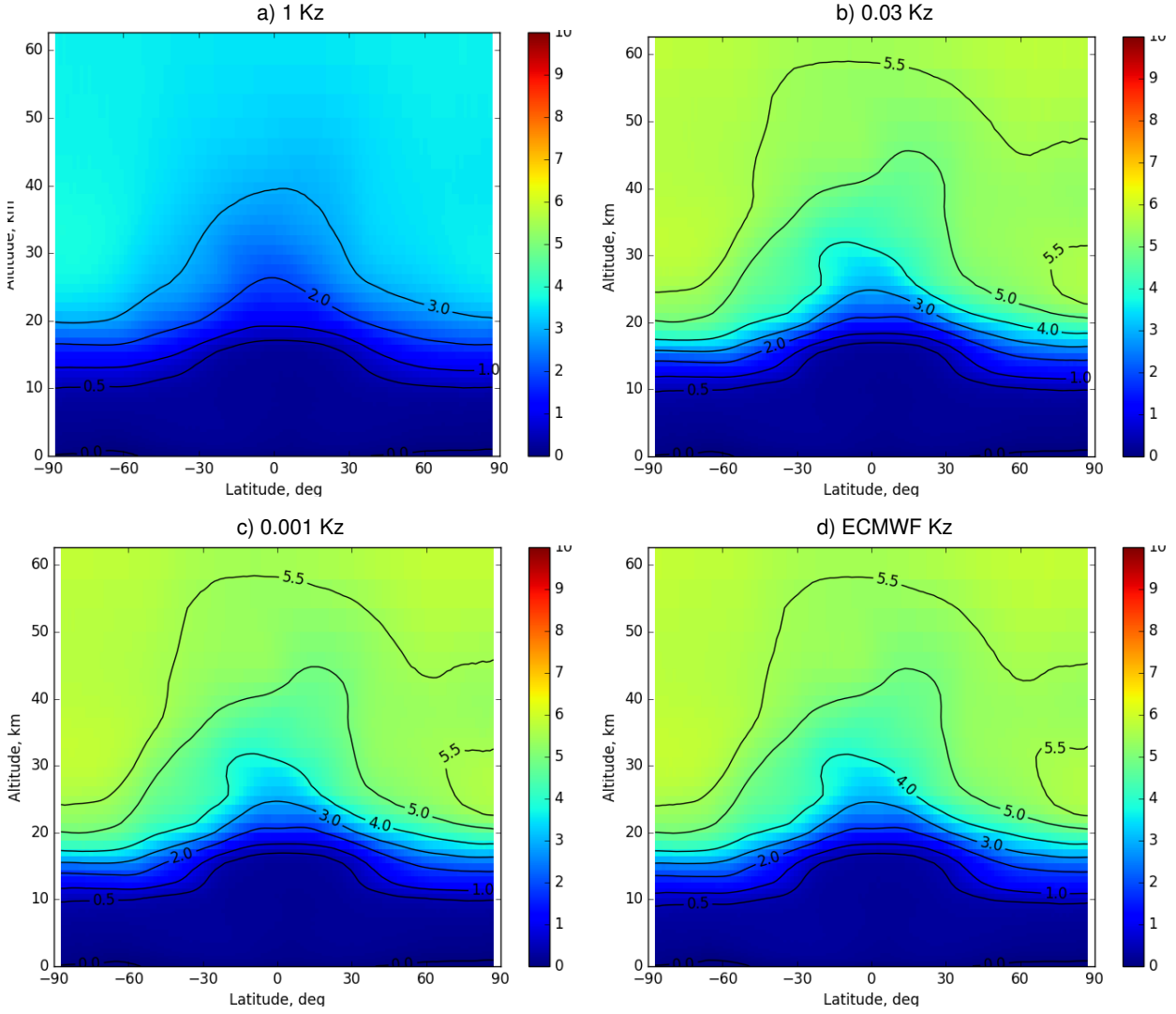

Figure 10. The zonal-mean spatial distribution of the ideal-age AoA for 2011 calculated for different eddy-diffusivity profiles.

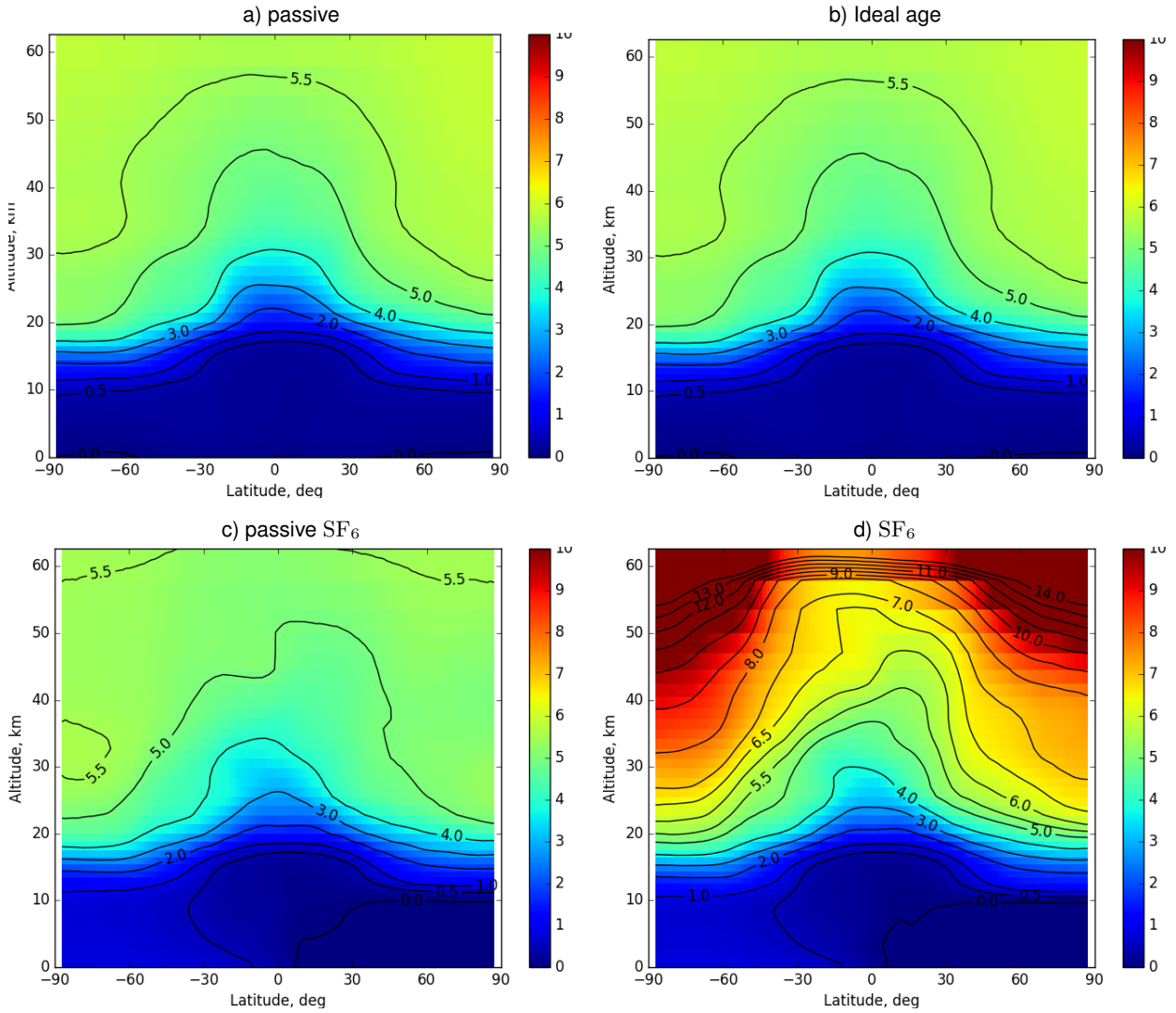

Figure 11. Zonal-mean distributions of atmospheric AoA simulated with "passive", ideal-age, and two SF_6 tracers, average for 2012.

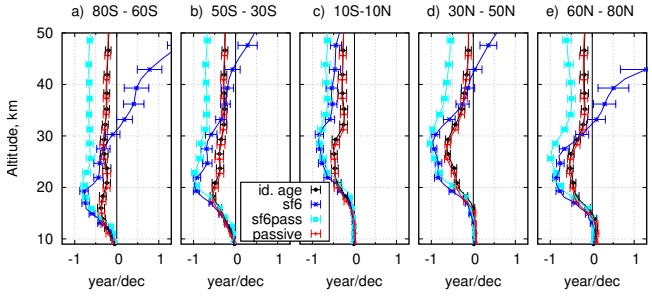

Figure 12. Vertical profiles of the simulated age of air linear trends over 11 years 2002-2012 for example latitude belts

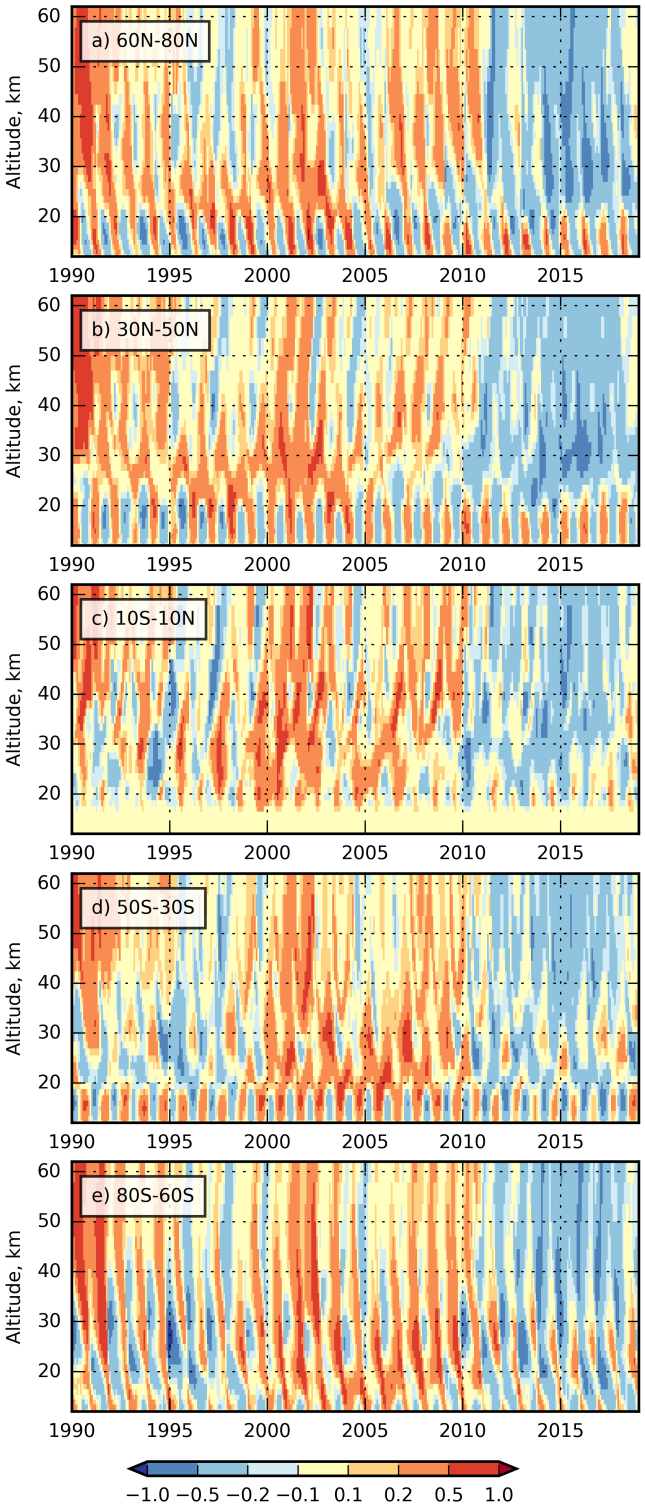

Figure 13. Anomaly of the ideal-age AoA (years) for the period of 1990-2018 with respect to the mean AoA

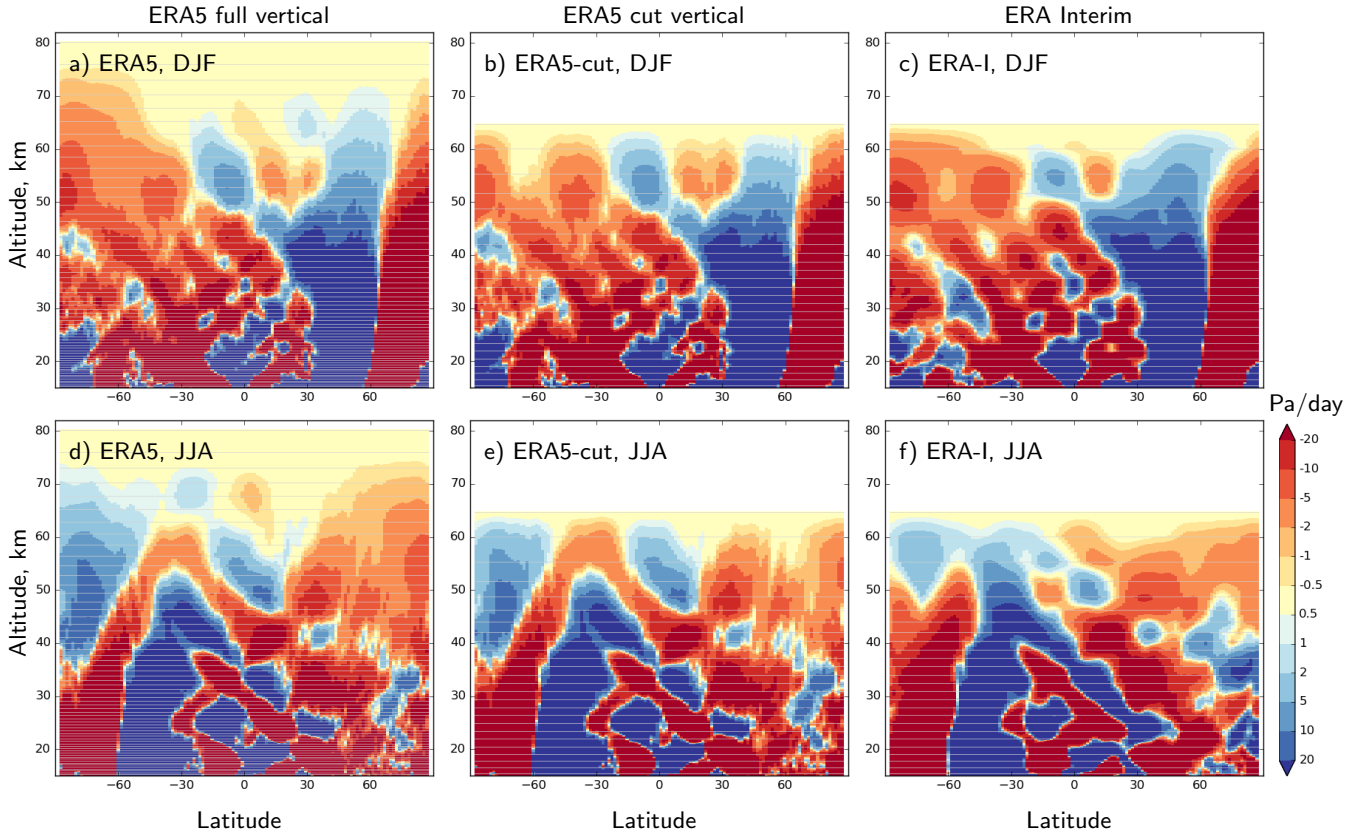

Figure 14. The seasonal and zonal-mean vertical air-mass fluxes diagnosed by SILAM from ERA5 and ERA-Interim fields for 2017 solstice seasons, expressed in terms of vertical velocity ω. Updrafts are red. The vertical-layers boundaries are shown with grey lines.